Available online at www.sciencedirect.com
ScienceDirect
Earth and Planetary Science Letters 256 (2007) 433–454
EPSL
www.elsevier.com/locate/epsl

Craton reactivation on the Labrador Sea margins: $^{40}Ar/^{39}Ar$ age and Sr–Nd–Hf–Pb isotope constraints from alkaline and carbonatite intrusives

Sebastian Tappe [a,*], Stephen F. Foley [b], Andreas Stracke [a,1], Rolf L. Romer [c], Bruce A. Kjarsgaard [d], Larry M. Heaman [e], Nancy Joyce [d]

[a] *Max-Planck-Institut für Chemie, Abteilung Geochemie, Postfach 3060, 55020 Mainz, Germany*
[b] *Institut für Geowissenschaften, Universität Mainz, Becherweg 21, 55099 Mainz, Germany*
[c] *GeoForschungszentrum Potsdam, Telegrafenberg, 14473 Potsdam, Germany*
[d] *Geological Survey of Canada, 601 Booth Street, Ottawa, Ontario, Canada K1A 0E8*
[e] *Department of Earth and Atmospheric Sciences, University of Alberta, 1-26 Earth Sciences Building, Edmonton, Alberta, Canada T6G 2E3*

Received 12 October 2006; received in revised form 29 January 2007; accepted 29 January 2007
Available online 6 February 2007
Editor: R.W. Carlson

Abstract

The once-contiguous North Atlantic craton (NAC) is crosscut by the Labrador Sea that opened during the Early Cenozoic after extensive Mesozoic continental rifting and removal of cratonic mantle. This large-scale structural change within the cratonic lithosphere was followed at about 150 Ma by the cessation of ultrapotassic and potassic-to-carbonatitic magma production, which had prevailed throughout much of the NAC history. At Aillik Bay, a sequence of olivine lamproites (1374.2±4.2 Ma, 2σ), aillikites/carbonatites (590–555 Ma), and nephelinites (141.6±1.0 Ma, 2σ) erupted through the southern NAC edge on the present-day Labrador Sea margin. Links between these alkaline magma types with diverse petrogeneses as a consequence of large-scale processes in the lithospheric mantle over a period of 1200 Myr are demonstrated utilizing their Sr–Nd–Hf–Pb isotope compositions.

The Mesoproterozoic olivine lamproites are characterized by unradiogenic Nd ($\varepsilon_{Nd(i)}$=−8.4 to −5.4), Hf ($\varepsilon_{Hf(i)}$=−11 to −7.8), and Pb ($^{206}Pb/^{204}Pb_{(i)}$=14.2–14.8) but moderately radiogenic Sr isotope compositions ($^{87}Sr/^{86}Sr_{(i)}$=0.7047–0.7062) fingerprinting long-term enriched cratonic mantle, which must have reached to depths of more than 150 km at this time. In contrast, Neoproterozoic carbonate-rich aillikites and carbonatites have fairly radiogenic Nd ($\varepsilon_{Nd(i)}$=0.1–1.8), Hf ($\varepsilon_{Hf(i)}$=−0.9 to +2.6), and Pb ($^{206}Pb/^{204}Pb_{(i)}$=17.5–18.8) but unradiogenic Sr isotope compositions ($^{87}Sr/^{86}Sr_{(i)}$=0.7033–0.7046) that point to the involvement of convective upper mantle material during melting. Simple binary mixing calculations coupled with the observation that carbonate-rich magmatism prevailed for over 30 Myr in the area imply a complex pattern of lithosphere–asthenosphere interaction at depths between ~180 and 140 km. The Cretaceous nephelinites have slightly unradiogenic Nd ($\varepsilon_{Nd(i)}$=−4 to −1.4), moderately radiogenic initial $^{87}Sr/^{86}Sr$ (0.7044–0.7062), but initial ε_{Hf} (−3.3 to +1.4) similar to the aillikites and highly radiogenic Pb ($^{206}Pb/^{204}Pb_{(i)}$=19.1–20.2) isotope compositions. Their sodic mafic alkaline nature reflects partial melting at a higher level of

* Corresponding author. Department of Earth and Atmospheric Sciences, University of Alberta, 1-26 Earth Sciences Building, Edmonton, Alberta, Canada T6G 2E3. Tel.: +1 780 4927225; fax: +1 780 4922030.
E-mail address: sebastian.tappe@ualberta.ca (S. Tappe).
[1] Now at: Institut für Isotopengeologie und Mineralische Rohstoffe, Department of Earth Sciences, ETH-Zürich, Clausiusstrasse 25, CH-8092 Zürich, Switzerland.

0012-821X/$ - see front matter
doi:10.1016/j.epsl.2007.01.036

the cratonic mantle tapping metasomatic components that had been introduced during the >30 Myr of Neoproterozoic aillikite/carbonatite magmatism.

The new $^{40}Ar/^{39}Ar$ age and Sr–Nd–Hf–Pb isotope data, along with petrological arguments, suggest that at least 30 km of the cratonic mantle beneath the southern NAC edge had been replaced by the hotter upwelling asthenosphere between ca. 550 Ma, when a thick diamond-bearing lithosphere was present, and 150 Ma. This lithospheric thinning presumably occurred shortly prior to Cretaceous continental rifting in response to enhanced plate-tectonic stresses focused at this zone of persistent lithospheric weakness. It appears, however, that the recurrent volatile-rich alkaline magmatism and associated mantle metasomatism played an important role in destroying the structural integrity of the cratonic mantle thereby aiding the subsequent lithosphere thinning.

Keywords: aillikite; carbonatite metasomatism; lamproite; lithosphere thinning; nephelinite; North Atlantic craton

1. Introduction

Cratons are crustal domains that have remained stable since the Early Precambrian and now form continental nuclei. Their apparent stability with long preservation of ancient felsic crust has been demonstrated to be linked to the composition and structure of the underlying lithospheric mantle roots [1–3]. These cratonic roots may reach to depths of more than 200 km and have been depleted in melt and dehydrated during Archean geodynamic processes [4]. They are chemically buoyant and highly viscous, and are able to reside in a dynamic mantle for billions of years [5]. However, this paradigm is in conflict with cratonic lithosphere reactivation being increasingly recognized as an alternative process that shapes the continents [6–10]. The best documented example for removal of ancient lithosphere is the North China craton where Archean crust is underlain by young and hot oceanic-type mantle [6,11,12]. A case for even more advanced cratonic lithosphere destruction can be made for the separated North Atlantic craton (NAC; Fig. 1), with remnants being preserved in West Greenland and coastal Labrador [13,14]. The NAC has experienced several aborted rifting events since Mesoproterozoic time ([10] and references therein), but convective thinning of the cratonic lithospheric mantle culminated during the Early Cenozoic opening of the Labrador Sea followed by a short period of ocean floor formation [15,16].

The West Greenland margin of the Labrador Sea rift has been known for the recurrence of deep alkaline magma production for 15 yrs, and this was explained in terms of zones of persistent lithospheric weakness spatially controlling the magmatism [17]. This is further substantiated by recent discoveries of analogue alkaline rock associations at the conjugate Canadian margin, which precisely fit into this temporal pattern [10,18–21]. To date, Mesoproterozoic lamproites (ca. 1400–1200 Ma), Neoproterozoic ultramafic lamprophyres (UML) plus related carbonatites (ca. 610–550 Ma), and Cretaceous mafic alkaline rock suites (ca. 150–100 Ma) have been found forming dyke swarms or central-complex intrusions on either side of the Labrador Sea (Fig. 1). However, the Aillik Bay locality at the central Labrador coast is unique in that all three magmatic pulses have been identified cutting through the NAC crust in a small area [10].

We have undertaken a $^{40}Ar/^{39}Ar$ geochronology, chemical, and Sr–Nd–Hf–Pb isotope study on the lamproites, UMLs/carbonatites, and mafic alkaline rock suites from the Aillik Bay area in an attempt to understand the nature and evolution of their source regions. The time-integrated isotope data, combined with findings from experimental petrology, allow evaluation of compositional and structural changes that occurred within the NAC mantle lithosphere before its break-up. Our proposed model suggests that at least 30 km of lithospheric mantle at the craton margin had been convectively removed by ca. 150 Ma, prior to the initiation of Cretaceous continental rifting that eventually led to sea-floor spreading in the Labrador Sea basin at ca. 60 Ma.

2. Geological background

2.1. Rifted North Atlantic craton

The Early Archean tonalitic crust of northern Labrador and western Greenland is among the oldest preserved on Earth [14]. It shares many compositional and structural features that allow assignment to a common Archean province [13,22]. This ancient micro-continent, which is commonly referred to as the North Atlantic craton (Fig. 1), was incorporated into the Laurentia plate assembly [23] during a sequence of subduction and collision events with neighbouring continental terrains between ca. 1900 and 1700 Ma [24]. The Paleoproterozoic collision zones are preserved

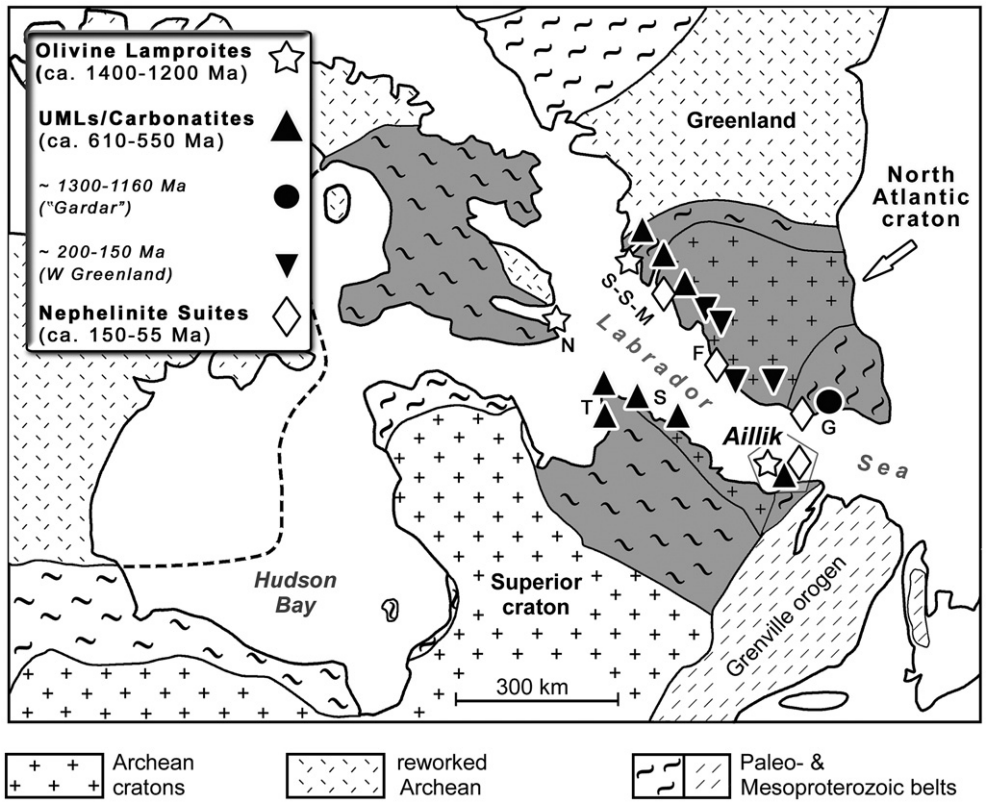

Fig. 1. Simplified geological map of the northeastern Canadian–Greenland Shield. The grey-shaded areas represent the North Atlantic craton with surrounding mobile belts on either side of the Labrador Sea. Note that only alkaline and carbonatite intrusives in the vicinity of the Labrador Sea are shown. The position of Greenland is restored for Cenozoic continental drift due to now extinct sea-floor spreading in the Labrador Sea (modified from [24]). Areas or locations mentioned in the text are abbreviated as follows: F – Frederikshåb Isblink; G – Gardar province; N – Napoleon Bay; S – Saglek block; SSM – Sisimiut–Sarfartoq–Maniitsoq areas; T – Torngat Mountains.

as circum-cratonic belts, along which the Archean crust had been reworked and juvenile components added.

Numerous rifting attempts are known to have affected the NAC since the Mesoproterozoic (Fig. 2); however, the region remained a coherent unit until ca. 140 Ma, when continental stretching led to the development of complex rift basins accommodating several thousand metres of clastic sediment [25]. Separation of the NAC was completed by Palaeocene sea-floor-spreading in the Labrador Sea at ca. 60 Ma [16]. While the deeply buried Late Mesozoic graben structures form part of the modern Labrador and Greenland shelves [15], the uplifted Precambrian basement blocks along these rifted margins record a protracted history of deep extension-related alkaline magmatism.

2.2. Recurrent alkaline magmatism

The margins of the Labrador Sea have been repeatedly subjected to melting events that produced comparatively small volumes of alkaline mafic/ultramafic and carbonatitic magma [17]. A marked correlation exists between the West Greenland and Canadian part of the rifted NAC in terms of the compositional and temporal patterns of the primitive alkaline magma types produced (Fig. 2). This correlation encompasses: (1) Mesoproterozoic lamproites, (2) Neoproterozoic UMLs/carbonatites, and (3) Cretaceous/Palaeogene melilitites, nephelinites, and basanites, which corresponds to a change in alkaline magma composition from ultrapotassic through carbonatitic–potassic to sodic alkaline over time. However, the ~30 by 30 km Aillik Bay area on the southern NAC edge is the only known occurrence where magmas of all three types and ages have erupted through the same crust [10].

UML/carbonatites of Mesoproterozoic ('Gardar' [26]) and Jurassic ages [17,27–29] have so far only been recorded from SW Greenland, but not from Labrador (Fig. 2). Nevertheless, the fact that ultrapotassic (ca. 1400–1200 Ma) and potassic-to-carbonatitic magma production (ca. 1300–1160 Ma; ca. 610–550 Ma; and ca. 200–150 Ma), which had prevailed throughout much of the NAC history, ceased relatively

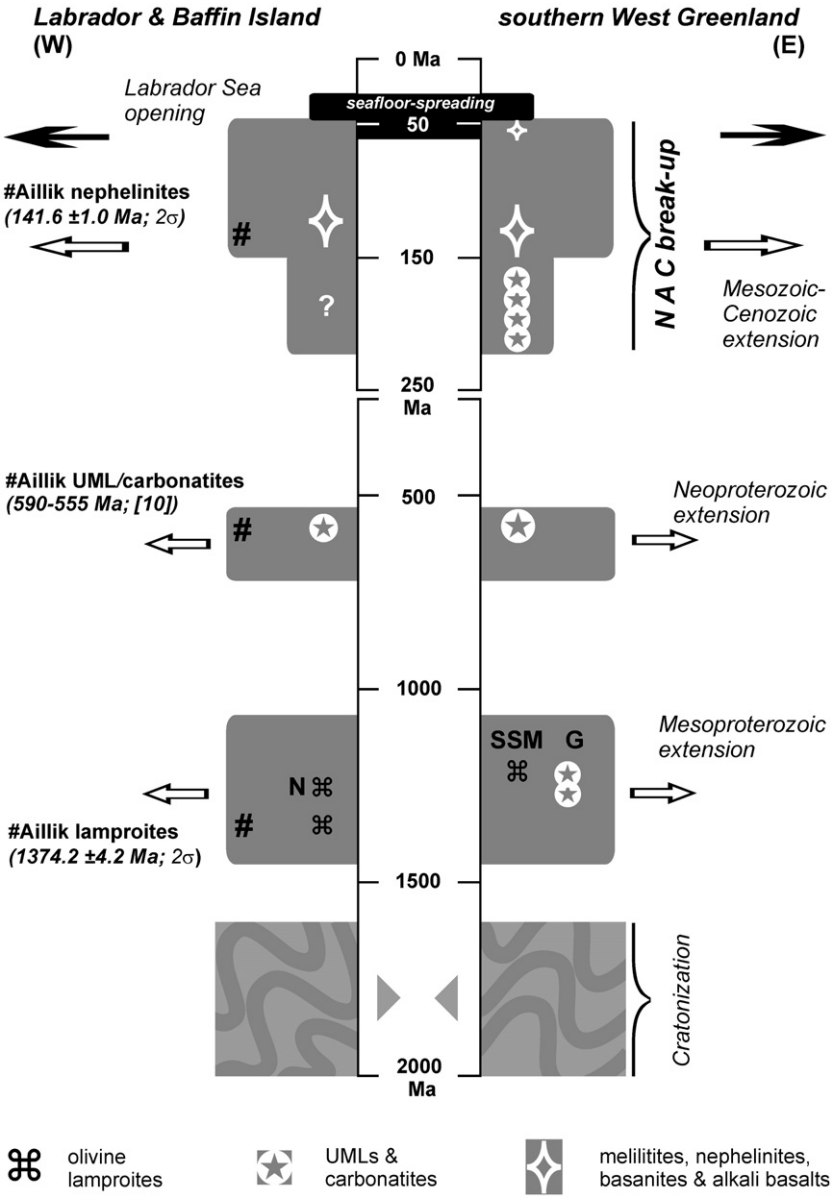

Fig. 2. 'Young' continental extension-related alkaline and carbonatite magmatism at the Labrador Sea margins (< 1400 Ma). Note the scale-break at 250 Ma. Grey fields along with arrows denote pronounced extensional episodes recorded by prominent mafic dyke swarms and/or rift-related sediments. Age range compilation includes U–Pb perovskite and zircon, as well as $^{40}Ar/^{39}Ar$ mineral and bulk-rock data. K–Ar and Rb–Sr bulk-rock age data are included only where no other age determinations are available. Note the ages of the three contrasting alkaline rock associations from the Aillik Bay area on the central Labrador coast discussed in this paper. (G) – 'Gardar' alkaline intrusions including carbonatites and UMLs. (N) – Napoleon Bay lamproites. (SSM) – Sisimiut lamproites. Primary data sources and/or previous age compilations are from: [10,17–21,25–32,34,35]. Tectonic framework based on [16,23].

abruptly at ca. 150 Ma requires a large-scale structural change within the NAC lithosphere.

3. Sample description and new $^{40}Ar/^{39}Ar$ age constraints

Mineral compositional data and descriptions of the lamproites and nephelinites from the Aillik Bay area (coastal Labrador) are provided as Supplementary files A1–2. Argon isotopic data for groundmass phlogopite from two lamproites and one nephelinite sample are listed in Supplementary file B and the argon gas release spectra are shown in Fig. 3 (uncertainties are quoted at 2σ; for analytical details see Supplementary file C). The petrology of the UMLs/carbonatites, including their U–Pb perovskite intrusion ages, is discussed in [10].

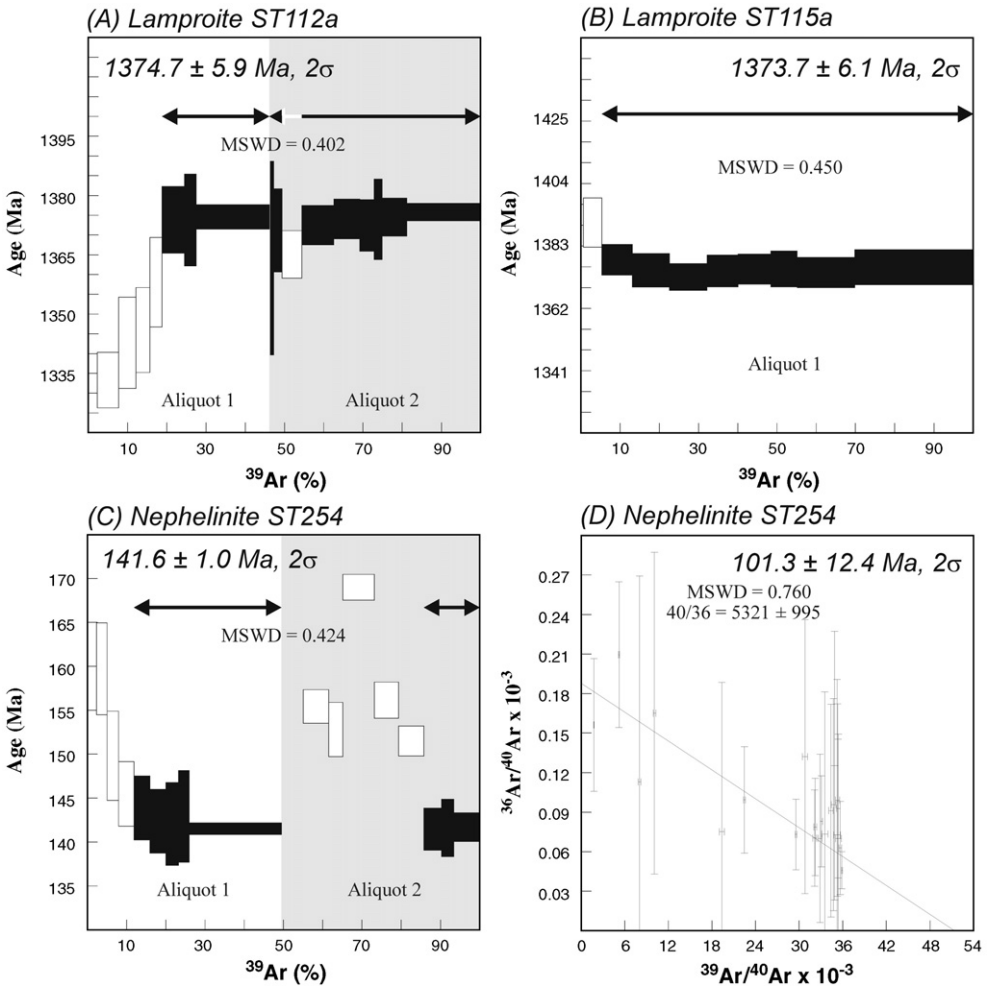

Fig. 3. Argon-release spectra of phlogopites from (A and B) Mesoproterozoic olivine lamproite dykes ST112a and ST115a, as well as from (C) Early Cretaceous nephelinite sill ST254. The inverse isochron in (D) includes all heating steps and passes through a $^{36}Ar/^{40}Ar$ value of 0.19×10^{-3} significantly lower than the atmospheric value (3.4×10^{-3}). This indicates degassing of weakly-bound excess ^{40}Ar from the phlogopite lattice during the early heating steps and therefore the combined multi-step plateau age in (C) is the more reliable emplacement age for nephelinite sill ST254.

3.1. Mesoproterozoic olivine lamproite dykes (ca. 1374 Ma)

Subvertical, fine-to medium-grained olivine lamproite dykes (0.2 to 2 m wide) can be traced for several hundred meters along strike (340° to 030°). The two analyzed phlogopite aliquots from olivine lamproite ST112a exhibit evidence for argon loss during the early heating steps. However, a well-defined multi-step plateau was obtained for each aliquot, yielding a combined plateau age of 1374.7±5.9 Ma (Fig. 3A; 75% of the total released ^{39}Ar). Phlogopite from olivine lamproite ST115a yielded a well-defined plateau age of 1373.7±6.1 Ma (Fig. 3B). The plateau was calculated over eight consecutive steps which contain 95% of the total released ^{39}Ar. The potential presence of excess argon was indicated during the two lowest temperature heating steps, which were not included in the plateau age calculation.

Taken together, the calculated weighted average age of 1374.2±4.2 Ma (1374.7±5.9 Ma and 1373.7±6.1 Ma) is considered the best estimate for olivine lamproite magmatism in the Aillik Bay area. This Mesoproterozoic lamproite melting event appears to represent the earliest of its kind on the fringes of the NAC (Fig. 1), with younger analogues occurring at Napoleon Bay on Baffin Island (1240±9 Ma; K–Ar phlogopite; [18]) and in the Sisimiut area of West Greenland (1227±12 Ma; Rb–Sr isochron; [30]).

3.2. Neoproterozoic UML/carbonatite dykes (ca. 590–555 Ma)

UML magma (aillikite and damtjernite) with associated carbonatite intruded between 590 and 555 Ma over a 35 Myr time span [10]. These pulses produced the largest volume of alkaline melt within the Aillik Bay area with the carbonate-rich members, the aillikites, being closest to primary magma composition [10]. Time equivalents occur in the Saglek area of northern Labrador (ca. 606–568 Ma; [21]), the Torngat Mountains of northern Labrador and New Quebec (ca. 600–550 Ma; [19–21]), and the Sisimiut–Sarfartoq–Maniitsoq areas of West Greenland (ca. 610–550 Ma; [30,31]).

3.3. Early Cretaceous nephelinite dyke suite (ca. 142 Ma)

Fine-grained olivine melilitite, nephelinite, and basanite form a suite of columnar jointed dykes and sills up to 2 m wide, preferentially oriented east–west. This silica-poor, Na-rich rock association is collectively referred to as the 'nephelinite suite'. The two analyzed phlogopite aliquots from nephelinite sill ST254 exhibit evidence for significant excess ^{40}Ar and apparently old ages in the lowest temperature heating steps. The higher temperature steps, however, yield a well-defined combined plateau age of 141.6±1.0 Ma (Fig. 3C; 52% of the total released ^{39}Ar). An inverse isochron that includes all heating steps gives an age of 101.3±12.4 Ma (Fig. 3D) and a ^{40}Ar/^{36}Ar value of 5321±995 is obtained, significantly higher than the atmospheric value (295.5). Therefore, we suggest that weakly-bound excess ^{40}Ar had degassed from the crystal lattice during the early heating steps and that the more precise combined higher temperature multi-step plateau age of 141.6±1.0 Ma is the most reliable crystallization age of nephelinite ST254. This Early Cretaceous age falls within a less well-constrained K–Ar bulk-rock age range of 145–129 Ma [32] that was determined on poorly described mafic dykes cutting a breccia bed at Ford's Bight in the Aillik Bay vicinity. The deposition age for this breccia was constrained by nannofossils to be Late Jurassic to Early Cretaceous [33]. Further occurrences of Early Cretaceous mildly alkaline basalts are known from deep wells drilled into the Labrador shelf (Alexis Formation; ca. 139–122 Ma; K–Ar bulk-rock; [32]). On the southern West Greenland margin (Fig. 1), the closest analogues of the Aillik Bay nephelinites are the coast-parallel alkaline basaltic dykes observed between 60 and 63°N (ca. 140–133 Ma; ^{40}Ar/^{39}Ar phlogopite; [28,34]) and a suite of melilitite to nephelinite dykes in the Frederikshåb Isblink area (ca. 152–115 Ma; K–Ar phlogopite, apatite fission-track, U–Pb perovskite, [28,35]).

4. Magma compositions

Representative bulk-rock chemical and the radiogenic isotope compositions are listed in Tables 1 and 2. Descriptions of the analytical techniques and the complete dataset are available online (Supplementary files C and D).

4.1. Major and compatible trace elements

The *olivine lamproites* are relatively SiO_2-poor (41.4–47 wt.%) and MgO-rich (6.1–13.1 wt.%; ST237=4.9 wt.%) which, in combination with elevated Ni (105–301 ppm) and Cr (183–464 ppm) concentrations, testifies to their mantle-derived nature. They are Al_2O_3 (8.2–9.8 wt.%) and CaO (6.3–10.1 wt.%) depleted, but strongly K_2O (3.9–7.3 wt.%; K_2O/Na_2O=2–5), TiO_2 (2.8–4.8 wt.%), and P_2O_5 (0.7–1.2 wt.%) enriched. CO_2 is elevated (1.2–5.1 wt.%) due to the presence of minor calcite in interstices and segregations.

The *aillikites* have high MgO (15–21 wt.%), Ni (211–719 ppm), and Cr (520–734 ppm) contents and are close to primary magma composition, as opposed to the UML variant damtjernite. Furthermore, field relations and the δ^{13}C values of carbonates revealed aillikites to be parental to the carbonatites into which they locally grade [10]. Hence, only aillikite bulk-rock major and trace element compositions are used in comparisons herein. However, the radiogenic isotope composition of the entire Aillik Bay UML/carbonatite suite is presented in order to demonstrate derivation from a common parental magma, the proto-aillikite of [10]. Aillikites are strongly SiO_2 (18–27 wt.%), Al_2O_3 (2.5–3.5 wt.%), and Na_2O (<0.7 wt.%) depleted but CaO (14–20 wt.%) and TiO_2 (2.5–4.8 wt.%) rich. High CO_2 (10–14 wt.%) and P_2O_5 (1.5–3 wt.%), and elevated K_2O (1.4–2.1 wt.%) content reflects their carbonatite affinity [36,37].

The *nephelinite suite* represents a more common type of rift-related mafic alkaline magma. Olivine melilitite ST103, nephelinites, and basanites are SiO_2-poor (34.7–44.3 wt.%) and have high MgO (6.9–11.3 wt.%), Ni (76–198 ppm), and Cr contents (123–485 ppm), consistent with primitive mantle-derived magmas. Na_2O (2–4 wt.%) dominates over K_2O (1.3–2 wt.%; $K_2O/Na_2O \leq 0.6$) and the Al_2O_3 (10.7–14.3 wt.%) contents approach basaltic levels. CaO (10.1–14.6 wt.%), TiO_2 (1.7–2.6 wt.%), and

Table 1
Major (wt.%) and trace element (ppm) concentrations of lamproites, aillikites, and nephelinite suite rocks from Aillik Bay, central Labrador coast

Rock type	Olivine lamproites				Ultramafic lamprophyres (UML)*				Nephelinite suite			
					Aillikites			Mela-aillikite	Mel	Neph	Bas	Neph
Sample No.:	ST112a	ST115a	ST223	L68	ST109	ST198a	ST250a	ST147b	ST103	ST241b	ST245	ST254
SiO_2	41.4	45.1	45.7	45.3	18.2	26.8	22.5	31.6	34.7	39.0	43.9	37.2
TiO_2	2.79	4.05	3.47	4.07	3.55	3.76	2.49	5.76	2.21	2.63	1.96	2.23
Al_2O_3	8.21	8.78	9.76	8.91	2.80	3.47	3.13	3.97	10.7	13.3	14.3	11.3
$Fe_2O_3^T$	12.4	12.4	11.2	12.0	16.0	13.7	12.2	17.5	11.8	12.5	11.5	11.6
MnO	0.15	0.12	0.13	0.13	0.25	0.20	0.23	0.19	0.27	0.22	0.18	0.19
MgO	13.1	8.88	8.05	8.22	15.9	17.3	20.4	16.8	9.72	6.94	8.13	11.0
CaO	10.1	7.16	7.81	6.83	19.7	14.3	15.6	11.0	12.1	10.8	10.1	14.6
Na_2O	1.71	1.33	2.37	1.70	0.15	0.71	0.18	0.63	2.96	3.90	3.70	3.04
K_2O	3.93	6.37	5.07	6.54	1.79	1.68	2.06	1.92	1.64	1.99	1.69	1.47
P_2O_5	0.74	1.09	0.86	1.15	3.06	1.70	1.49	1.34	2.53	1.05	0.69	1.15
H_2O**	2.83	1.95	1.30	1.02	3.84	1.71	4.67	3.38	6.43	1.87	1.39	1.55
CO_2	1.47	1.21	3.50	2.02	13.5	13.3	13.8	4.60	3.70	4.50	1.54	3.75
Total	98.9	98.4	99.1	97.9	98.7	98.6	98.7	98.6	98.7	98.7	99.1	99.1
LFSE												
Cs	4.96	2.67	2.36	1.86	1.53	1.23	6.13	1.56	8.81	16.0	4.65	0.65
Rb	112	120	107	121	61.0	48.9	74.9	48.6	48.0	63.6	44.5	35.9
Ba	2210	2662	2360	3741	2777	1028	1366	594	2327	1408	1346	1169
Sr	1473	1156	1403	2161	1678	1318	1312	1330	1759	1797	1603	1455
HFSE												
Th	6.44	8.16	5.69	10.9	24.0	13.5	15.5	9.18	18.9	14.9	8.38	12.6
U	1.25	1.63	1.12	2.65	4.54	8.79	6.01	4.47	5.47	2.44	2.13	3.43
Nb	92.6	98.7	99.1	84.8	203	131	184	130	154	139	105	112
Ta	4.28	4.90	4.05	3.05	12.7	7.86	10.3	7.47	6.77	6.30	4.67	4.51
Pb	7.03	17.2	8.51	17.8	11.9	5.38	10.8	4.16	8.88	5.62	1.67	5.75
Zr	261	653	432	605	591	350	303	491	380	273	194	218
Hf	6.83	15.2	11.5	14.5	13.9	7.90	8.62	11.74	7.57	6.14	4.35	4.93
Y	19.9	27.9	21.2	30.2	42.8	34.7	27.1	35.4	41.6	42.0	23.3	26.2
REE												
La	73.0	121	87.9	129	390	182	242	116	214	123	97.1	115
Ce	142	259	179	269	819	391	476	268	416	233	177	221
Pr	16.2	31.6	20.9	32.8	95.8	45.9	52.4	32.7	45.7	24.6	18.4	23.8
Nd	66.6	124	79.9	128	364	181	188	134	175	88.1	64.3	90.5
Sm	12.7	19.9	14.1	20.3	54.6	31.3	28.1	25.8	28.6	15.2	10.7	14.7
Eu	3.82	5.87	4.06	5.98	13.5	8.45	7.14	7.16	7.61	4.49	3.24	4.31
Gd	9.48	13.1	9.64	13.4	33.4	21.5	17.4	19.2	20.0	11.5	7.87	10.8
Tb	1.13	1.58	1.18	1.62	3.30	2.43	1.91	2.24	2.37	1.58	1.06	1.34
Dy	5.01	7.31	5.08	7.65	12.8	9.80	7.70	9.47	10.1	7.85	5.00	6.14
Ho	0.74	1.13	0.80	1.23	1.65	1.30	1.11	1.31	1.48	1.53	0.87	1.04
Er	1.78	2.53	1.91	2.84	3.63	2.95	2.44	2.91	3.83	4.61	2.27	2.63
Tm	0.21	0.29	0.24	0.33	0.39	0.34	0.29	0.33	0.48	0.68	0.29	0.32
Yb	1.21	1.61	1.28	1.89	2.05	1.69	1.47	1.82	2.80	4.01	1.73	1.85
Lu	0.16	0.25	0.15	0.30	0.23	0.20	0.17	0.22	0.39	0.55	0.24	0.24
Transition metals												
Cr	464	266	333	245	520	726	734	705	213	123	238	259
Co	59.3	n.a.	44.5	35.0	61.6	73.5	63.3	91.5	45.7	38.8	41.4	45.1
Ni	301	236	218	217	211	509	487	593	157	75.5	149	172
Sc	21	n.a.	17	n.a.	28	20	21	23	24	17	20	27
V	185	n.a.	162	121	267	211	197	293	234	205	183	234

*Bulk-rock major and trace element data for damtjernites and carbonatites from the Neoproterozoic UML suite are published in Tappe et al. [10].
**Calculated difference of "loss on ignition" and CO_2 content; n.a. = not analyzed.

Table 2
Sr–Nd–Hf–Pb isotope composition of lamproites, UMLs/carbonatites, and nephelinite suite rocks from the Aillik Bay area, central Labrador coast

Sample No.:	$^{87}Sr/^{86}Sr_m$	$^{87}Sr/^{86}Sr_i$	$^{143}Nd/^{144}Nd_m$	$*(\varepsilon_{Nd})_i$	$**T^{Nd}_{(DM)}$	$^{176}Hf/^{177}Hf_m$	$*(\varepsilon_{Hf})_i$	$**T^{Hf}_{(DM)}$	$^{206}Pb/^{204}Pb_m$	$^{206}Pb/^{204}Pb_i$	$^{207}Pb/^{204}Pb_m$	$^{207}Pb/^{204}Pb_i$	$^{208}Pb/^{204}Pb_m$	$^{208}Pb/^{204}Pb_i$
Lamproites (1374 Ma)														
ST112a	0.710392(9)	0.70615	0.511631(8)	−5.4	2.2	0.281806(8)	−8.3	2.3	16.79	14.21	15.16	14.93	37.78	33.71
ST115a	0.710533(9)	0.70477	0.511431(7)	−6.1	2.1	0.281712(4)	−10.8	2.4	16.19	14.84	15.13	15.01	36.88	34.82
ST152b	0.708842(7)	0.70503	0.511526(6)	−6.9	2.3	0.281747(8)	−9.1	2.3	16.36	14.47	15.17	15.01	36.78	34.01
ST208	0.708828(7)	0.70493	0.511464(5)	−5.5	2.1	0.281728(5)	−9.4	2.3	16.10	14.78	15.10	14.99	36.34	34.37
ST223	0.708974(7)	0.70473	0.511397(6)	−8.4	2.3	0.281719(6)	−10.0	2.3	16.13	14.28	15.09	14.92	36.57	33.68
ST237	0.711040(7)	0.70560	0.511591(4)	−5.4	2.1	0.281775(7)	−7.8	2.2	18.01	17.11	15.34	15.26	37.33	36.35
L67	0.711208(7)	0.70475	0.511453(8)	−5.6	2.1	0.281701(7)	−11.0	2.4	17.54	14.76	15.18	14.94	37.54	34.49
L68	0.708201(7)	0.70507	0.511440(10)	−5.6	2.1	0.281721(7)	−10.9	2.4	16.30	14.17	15.10	14.92	37.02	34.35
UMLs/carbonatites (590–555 Ma)														
Aillikites														
ST109	0.704828(7)	0.70398	0.512253(3)	0.3	1.0	0.282495(7)	0.0	1.1	20.68	18.19	15.65	15.50	42.39	38.18
ST164	0.704497(7)	0.70394	0.512314(5)	0.6	1.1	0.282474(9)	−0.9	1.1	28.64	18.85	16.17	15.59	42.53	38.49
ST198a	0.704586(8)	0.70372	0.512313(6)	0.5	1.1	0.282516(6)	0.3	1.1	30.95	18.63	16.35	15.62	44.12	38.07
ST220II	0.704040(7)	0.70369	0.512313(5)	0.1	1.1	0.282547(15)	0.8	1.1	26.55	17.75	16.07	15.54	42.90	37.79
ST225	0.703999(7)	0.70376	0.512279(5)	0.9	1.0	0.282556(26)	1.2	1.1	n.a.	n.a.	n.a.	n.a.	n.a.	n.a.
ST250a	0.705223(10)	0.70389	0.512251(6)	0.3	1.0	0.282478(7)	−0.8	1.1	22.38	18.72	15.81	15.59	41.40	38.39
L60	0.704371(7)	0.70389	0.512264(5)	0.4	1.1	0.282475(5)	−0.9	1.1	27.36	17.68	16.08	15.50	41.67	37.58
Mela-aillikites														
ST147b	0.704654(10)	0.70380	0.512335(4)	0.1	1.2	0.282507(7)	0.3	1.1	26.05	18.47	16.05	15.60	43.35	38.38
ST196	0.705967(7)	0.70325	0.512399(5)	1.0	1.1	0.282512(11)	0.6	1.1	n.a.	n.a.	n.a.	n.a.	n.a.	n.a.
ST244b	0.705726(7)	0.70455	0.512419(5)	1.8	1.0	0.282578(3)	2.6	1.0	29.59	17.91	16.22	15.52	45.40	37.61
Damtjernites														
ST140	0.704384(7)	0.70357	0.512446(5)	1.4	1.1	0.282543(9)	1.6	1.0	28.30	18.57	16.12	15.54	42.80	37.85
ST174	0.704304(7)	0.70397	0.512372(8)	0.8	1.1	0.282517(5)	0.7	1.1	n.a.	n.a.	n.a.	n.a.	n.a.	n.a.
ST188a	0.703984(7)	0.70360	0.512402(4)	0.9	1.1	0.282560(6)	1.5	1.1	22.92	18.03	15.79	15.50	41.49	37.88
ST206aI	0.704729(7)	0.70377	0.512402(5)	1.5	1.1	0.282540(5)	1.3	1.0	24.07	17.76	15.84	15.46	46.40	38.22
ST224b	0.704944(7)	0.70398	0.512375(8)	0.5	1.2	0.282525(15)	1.1	1.0	n.a.	n.a.	n.a.	n.a.	n.a.	n.a.
ST226	0.705013(10)	0.70392	0.512396(6)	1.6	1.0	0.282559(3)	1.9	1.0	22.17	18.39	15.71	15.49	45.03	39.13
ST246a	0.705594(7)	0.70443	0.512454(5)	1.1	1.2	0.282670(6)	2.3	1.2	n.a.	n.a.	n.a.	n.a.	n.a.	n.a.

ST256		0.707524(7)	0.70662	0.512435(5)	1.9	1.1	0.282558(8)	1.7	1.0	23.22	17.70	15.81	15.48	40.40	37.49
Dol carbonatites															
ST189		0.704168(7)	0.70399	0.512189(5)	1.3	0.9	n.a.	n.a.	n.a.	18.36	17.52	15.51	15.46	39.96	35.25
ST203		0.705026(7)	0.70466	0.512188(5)	1.2	0.9	n.a.	n.a.	n.a.	19.26	18.39	15.59	15.53	41.91	36.29
L1		0.704472(7)	0.70421	0.512109(4)	0.6	0.9	n.a.	n.a.	n.a.	26.15	18.07	16.03	15.55	43.32	39.07
Dol-cal carbonatites															
ST126		0.707782(7)	0.70579	0.512224(6)	0.3	1.0	0.282511(12)	−3.7	1.6	n.a.	n.a.	n.a.	n.a.	n.a.	n.a.
ST193a		0.704094(7)	0.70393	0.512282(6)	0.6	1.0	0.282826(56)	6.5	1.0	n.a.	n.a.	n.a.	n.a.	n.a.	n.a.
ST198c		0.703967(7)	0.70389	0.512300(5)	0.6	1.1	0.282614(8)	0.3	1.3	21.90	17.49	15.80	15.54	43.73	36.83
ST199		0.704142(7)	0.70394	0.512295(5)	0.8	1.0	n.a.	n.a.	n.a.	25.91	18.35	16.07	15.62	40.04	38.44
ST231a		0.706439(7)	0.70429	0.512371(5)	0.6	1.2	0.282643(6)	2.3	1.1	27.75	17.77	16.07	15.48	44.28	35.49
Nephelinite suite (142 Ma)															
ST100	*Nephelinite*	0.705029(23)	0.70469	0.512371(10)	−3.4	1.0	0.282773(8)	−0.1	0.8	20.84	20.02	15.64	15.60	40.42	39.53
ST102	*Basanite*	0.705085(7)	0.70491	0.512358(6)	−3.6	0.9	0.282689(7)	−3.3	1.1	20.54	20.00	15.63	15.60	40.06	39.47
ST103	*Melilitite*	0.706340(7)	0.70618	0.512341(4)	−4.0	1.0	0.282637(6)	−4.7	1.0	20.30	19.39	15.59	15.55	40.14	39.11
ST217	*Basanite*	0.704517(7)	0.70435	0.512458(6)	−1.8	0.9	0.282760(12)	−0.4	0.8	20.13	19.47	15.63	15.60	40.64	39.53
ST241b	*Nephelinite*	0.705049(8)	0.70485	0.512471(6)	−1.6	0.9	0.282814(6)	1.0	0.8	20.12	19.48	15.61	15.58	40.77	39.48
ST245	*Basanite*	0.705527(7)	0.70537	0.512477(4)	−1.4	0.9	0.282812(14)	1.4	0.7	21.38	19.45	15.68	15.59	40.73	38.24
ST253	*Nephelinite*	0.705816(7)	0.70558	0.512445(4)	−2.1	0.9	0.282787(7)	0.7	0.7	19.83	19.08	15.57	15.53	40.08	39.46
ST254	*Nephelinite*	0.705335(7)	0.70519	0.512461(4)	−1.7	0.9	0.282802(12)	1.1	0.7	21.12	20.21	15.66	15.62	41.14	40.05
L59	*Nephelinite*	0.704606(8)	0.70444	0.512475(6)	−1.4	0.8	0.282761(9)	−0.4	0.8	20.67	19.44	15.62	15.56	40.34	39.53

Initial values calculated for emplacement ages of 1374 Ma (lamproites), 582 Ma (UMLs/carbonatites), and 142 Ma (nephelinite suite) using ^{87}Rb $1.42 * 10^{-11}$ y^{-1}, ^{147}Sm $6.54 * 10^{-12}$ y^{-1}, ^{176}Lu $1.865 * 10^{-11}$ y^{-1}, ^{232}Th $4.9475 * 10^{-11}$ y^{-1}, ^{235}U $9.848 * 10^{-10}$ y^{-1}, ^{238}U $1.55125 * 10^{-10}$ y^{-1} decay constants.

*Initial epsilon Nd and Hf values calculated using ^{147}Sm decay constant of $6.54 * 10^{-12}$ y^{-1} [$(^{143}Nd/^{144}Nd)_{CHUR}=0.512638$, $(^{147}Sm/^{144}Nd)_{CHUR}=0.1967$], and ^{176}Lu decay constant of $1.865 * 10^{-11}$ y^{-1} [$(^{176}Hf/^{177}Hf)_{CHUR}=0.282843$, $(^{176}Lu/^{177}Hf)_{CHUR}=0.0342$], respectively.

**Depleted Mantle model ages [$T^{Nd}_{(DM)}$] and [$T^{Hf}_{(DM)}$] calculated using ^{147}Sm decay constant of $6.54 * 10^{-12}$ y^{-1} [$(^{143}Nd/^{144}Nd)_{DM}=0.513150$ and $(^{147}Sm/^{144}Nd)_{DM}=0.222$], and ^{176}Lu decay constant of $1.865 * 10^{-11}$ y^{-1} [$(^{176}Hf/^{177}Hf)_{DM}=0.283150$ and $(^{176}Lu/^{177}Hf)_{DM}=0.034$], respectively.

Numbers in parentheses are 2-sigma errors of the mean for individual isotope ratio measurements; n.a. = not analyzed.

CO_2 (0.3–4.5 wt.%) are variable, falling at the high-end of the compositional spectrum covered by continental mafic alkaline rocks as expressed by conspicuously elevated CaO/Al_2O_3 ratios (1.0±0.2).

4.2. Incompatible trace elements

Primitive upper mantle (PUM; [38]) normalized incompatible element abundance patterns are displayed in Fig. 4. The *lamproites* show a strong low field strength element (LFSE) enrichment with Cs, Rb, Ba, and K approaching concentration levels of 400×PUM. The highly incompatible high field strength elements (HFSE) Th and U show strong relative depletions if compared to neighbouring Ba and Nb. This results in extremely high Nb/U ratios (74–89; ST237=41.7), significantly higher than for average continental crust (ca. 8–12) and oceanic basalts (47±10). Relative depletions also occur at Pb and P; only one lamproite (ST237) exhibits a positive spike at Pb and seems to have interacted with continental crust material (see also lower Nb/U and higher Pb isotope ratios). The Zr and Hf concentrations of the lamproites are high approaching 688 and 20 ppm, respectively; Zr/Nb ratios (4.3–9.5) are the highest amongst the three described alkaline rock suites. The light rare earth elements (LREE) are

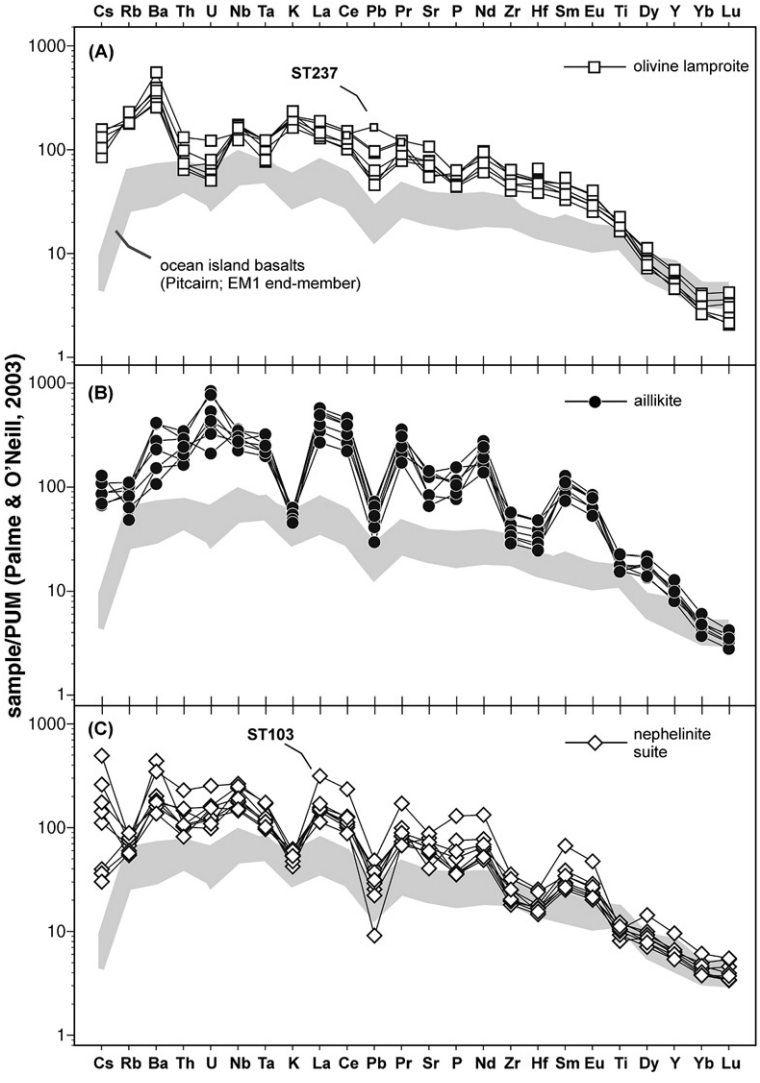

Fig. 4. Primitive upper mantle-normalized (PUM) incompatible element distribution for (A) Mesoproterozoic olivine lamproites, (B) Neoproterozoic aillikites, and (C) members of the Cretaceous nephelinite suite from the Aillik Bay area. Grey-shaded fields indicate a typical 'Enriched Mantle' derived oceanic island basalt trace element pattern for comparison [77]. Note the overall similarity between aillikite and nephelinite patterns. PUM values are from [38].

moderately enriched (up to 200×PUM), whereas the heavy REE (HREE) are strongly depleted, falling below 4×PUM with La/Yb_{CN}=37–57.

Aillikites show extreme Ba, Th, U, Nb, Ta, and LREE concentration levels exceeding 200×PUM. However, the PUM-normalized patterns are deeply dissected, indicating strong incompatible element fractionation during melting [10]. Pronounced relative depletions are apparent at Rb, K, Pb, Sr–P, Zr–Hf, and the HREE, which can be as low as 3×PUM. REE fractionation is extreme (La/Yb_{CN}=66–130) and strong incompatible element enrichment is furthermore evident from the subchondritic Zr/Nb (1.6–2.9) and Nb/U (9–31), indicative of a pronounced U-enrichment.

Interestingly, the *nephelinite suite* shows a PUM-normalized incompatible element distribution reminiscent of the aillikites, although concentration levels are less extreme. For example, the HFSE (Th, U, Nb, Ta, Zr, Hf) and LREE abundances are much lower than in aillikites, but the Zr/Nb ratios (1.5–3.0) are identical. Furthermore, the LFSE are moderately enriched and show the same relative depletions at Rb and K as aillikites. The same holds true for the troughs at Pb and Zr–Hf, although only the nephelinite suite has consistently suprachondritic Zr/Hf ratios (42–59) as opposed to near-chondritic ratios in lamproites (35–43) and aillikites (35–44). The LREE are enriched over the HREE (La/Yb_{CN}=20–52), but

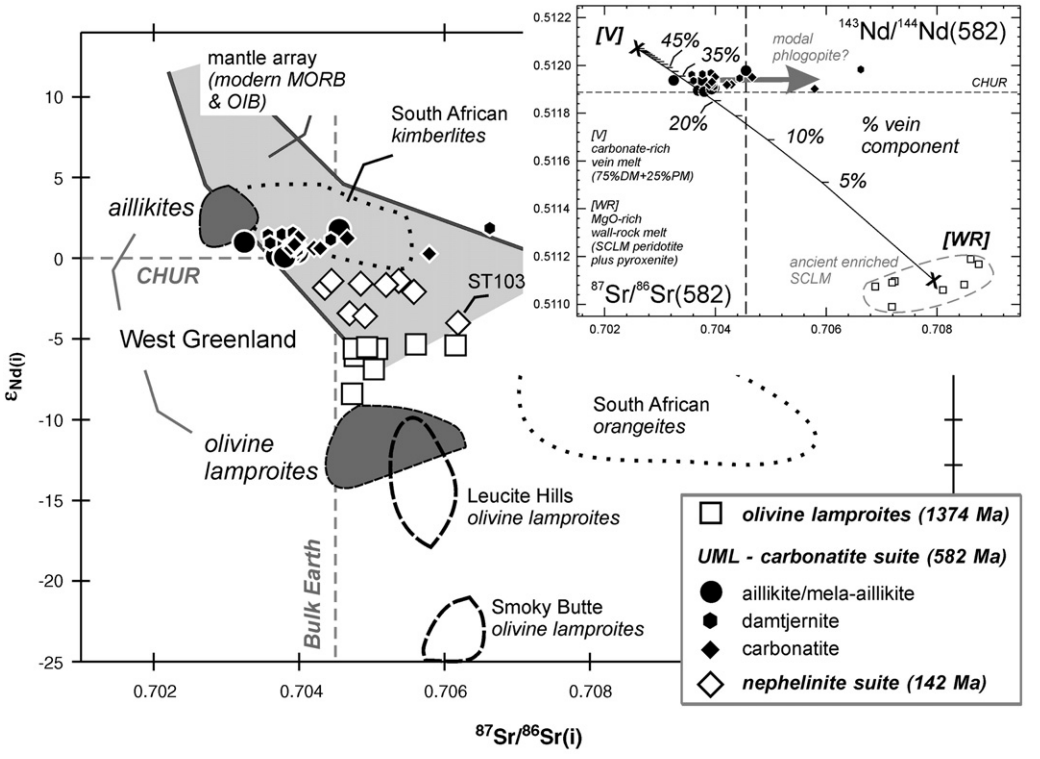

Fig. 5. $\varepsilon_{Nd(i)}$ vs $^{87}Sr/^{86}Sr_{(i)}$ for Mesoproterozoic olivine lamproites, Neoproterozoic UMLs/carbonatites, and members of the Cretaceous nephelinite suite from the Aillik Bay area. The inset shows a mixing hyperbola constructed between *[V]* carbonate-rich vein and *[WR]* MgO-rich wall-rock melt components. The vein melt is assumed to have formed by a two-stage process at the base of the cratonic SCLM that includes (1) the infiltration and solidification of initial CO_2-rich low-degree melt from convective mantle material (75% Depleted Mantle plus 25% Primitive Mantle; $^{87}Sr/^{86}Sr_{(582)}$=0.702589; $^{143}Nd/^{144}Nd_{(582)}$=0.51207) and (2) its remobilization as 'carbonatitic' melt (Sr=5500 ppm; Nd=350 ppm) triggering volatile-fluxed melting of the SCLM wall-rocks. The wall-rock melt is assumed to have formed by 10% of partial melting of long-term enriched SCLM garnet peridotite containing subordinate mica clinopyroxenite residues (the inferred lamproite source region aged to 582 Ma; $^{87}Sr/^{86}Sr_{(582)}$=0.707931; $^{143}Nd/^{144}Nd_{(582)}$=0.511103; Sr=480 ppm; Nd=25.3 ppm). The mixing relations illustrate that the Sr–Nd isotope compositions of aillikites (close to Bulk Earth) can be produced by adding only 20 to 40% of isotopically mildly depleted carbonate vein melt into MgO-rich melts derived from long-term enriched SCLM. This mixing proportion is also in keeping with the major and trace element characteristics of aillikites. Note the horizontal trend towards radiogenic Sr can be produced by enhanced radiogenic in-growth due to phlogopite in the vein and wall-rock component with high Rb/Sr [10]. Fields for West Greenland aillikites and olivine lamproites [39], Leucite Hills and Smoky Butte olivine lamproites [57,62], and South African kimberlites and orangeites [78] are shown for comparison.

to a smaller extent as compared to the lamproite and aillikite data. Nb/U ratios (28–60) are similar to oceanic basalts (47±10).

4.3. Radiogenic isotopes

The *lamproites* have low initial ε_{Nd} (−8.4 to −5.4; Fig. 5) and ε_{Hf} (−11 to −7.8; Fig. 6) values at only moderately radiogenic Sr isotope compositions ($^{87}Sr/^{86}Sr_{(i)}$=0.70473–0.70615; Fig. 5). They have some of the most unradiogenic $^{206}Pb/^{204}Pb_{(i)}$ (14.2–14.8; ST237=17.1), $^{207}Pb/^{204}Pb_{(i)}$ (14.9–15.0; ST237=15.3), and $^{208}Pb/^{204}Pb_{(i)}$ (33.7–34.4; ST237=36.4) ratios among alkaline rocks worldwide, but importantly they overlap the Pb isotope composition of their West Greenland analogues from Sisimiut (Fig. 7; [39]).

Aillikites are characterized by $\varepsilon_{Nd(i)}$ (+0.1 to +1.8) and $\varepsilon_{Hf(i)}$ (−0.9 to +2.6) close to Bulk Earth. Their Sr isotope composition is the least radiogenic ($^{87}Sr/^{86}Sr_{(i)}$= 0.70325–0.70455) among the Aillik Bay alkaline rock suites. They have variable but moderate $^{206}Pb/^{204}Pb_{(i)}$ (17.7–18.8), $^{207}Pb/^{204}Pb_{(i)}$ (15.5–15.6), and $^{208}Pb/^{204}Pb_{(i)}$ (37.7–38.5) ratios compared with lamproites and the highly radiogenic Pb isotope composition of the *nephelinite suite* ($^{206}Pb/^{204}Pb_{(i)}$=19.1–20.2; $^{207}Pb/^{204}Pb_{(i)}$= 15.5–15.6; $^{208}Pb/^{204}Pb_{(i)}$=38.2–40.1; Fig. 7). The members of the nephelinite suite have negative $\varepsilon_{Nd(i)}$ (−3.6 to −1.4; ST103=−4.0); however, $\varepsilon_{Hf(i)}$ values (−3.3 to +1.4; ST103=−4.7) are close to Bulk Earth (Fig. 6). The $^{87}Sr/^{86}Sr_{(i)}$ (0.70435–0.70558; ST103=0.70618) ratios are moderately radiogenic. While the olivine melilitite ST103 represents an end-member composition in Sr–Nd–Hf isotope space, it falls within the Pb

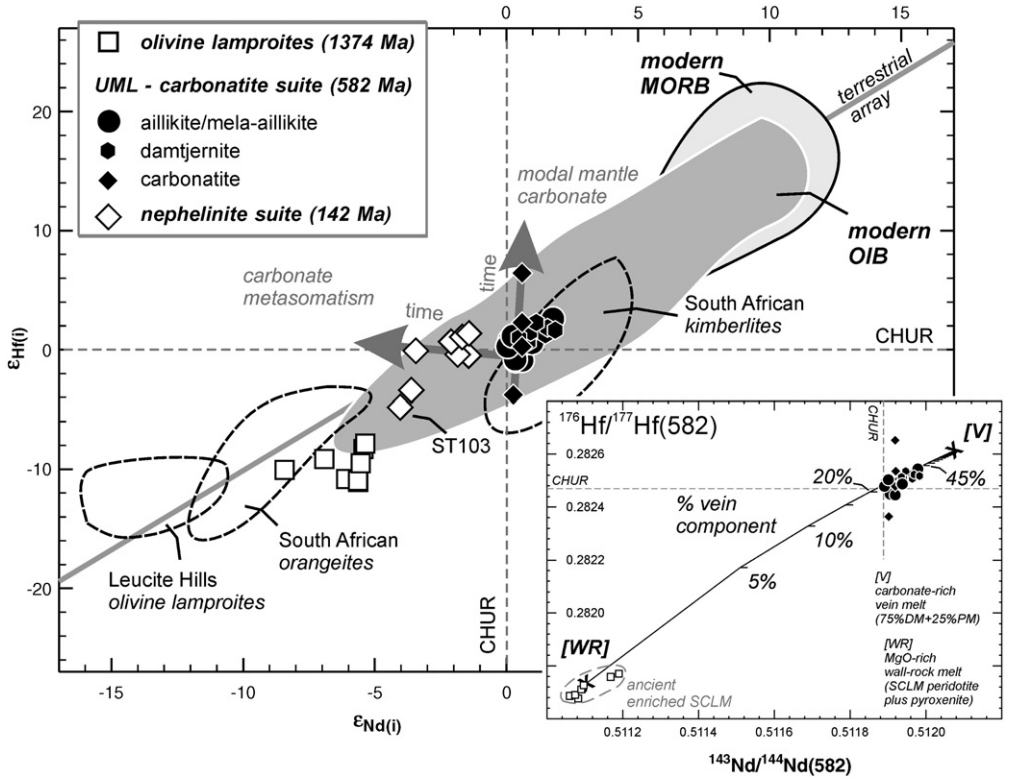

Fig. 6. $\varepsilon_{Hf(i)}$ vs $\varepsilon_{Nd(i)}$ for Mesoproterozoic olivine lamproites, Neoproterozoic UMLs/carbonatites, and members of the Cretaceous nephelinite suite from the Aillik Bay area. The inset shows a mixing hyperbola constructed between *(V)* carbonate-rich vein and *(WR)* MgO-rich SCLM wall-rock melt components. The underlying modelling assumptions are described in the main text and in the caption to Fig. 5. *Carbonate-rich vein melt parameters:* $^{143}Nd/^{144}Nd_{(582)}$=0.51207; $^{176}Hf/^{177}Hf_{(582)}$=0.28261; Nd=350 ppm; Hf=40 ppm. *SCLM wall-rock melt parameters:* $^{143}Nd/^{144}Nd_{(582)}$=0.511103; $^{176}Hf/^{177}Hf_{(582)}$=0.281734; Nd=25.3 ppm; Hf=2.1 ppm. The two grey arrows illustrate likely effects of carbonate metasomatism (from aillikites towards nephelinites) and modal carbonation (the steep vector defined by the 4 carbonatites) of peridotite material over time (see details in [66]). Fields for South African kimberlites and orangeites [78], Leucite Hills olivine lamproites [79], and modern oceanic basalts (compilation of A. Stracke) are shown for comparison. Terrestrial array after [65].

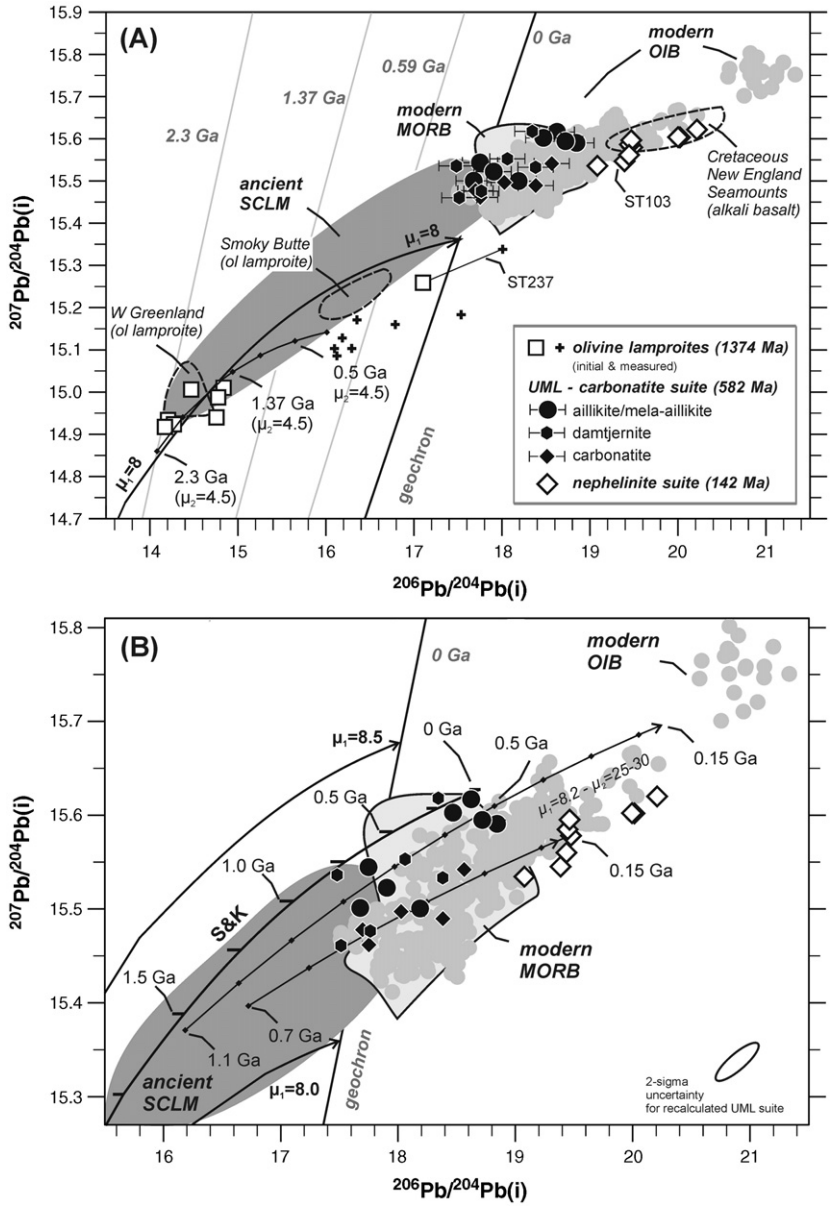

Fig. 7. $^{207}Pb/^{204}Pb_{(i)}$ vs $^{206}Pb/^{204}Pb_{(i)}$ for Mesoproterozoic olivine lamproites, Neoproterozoic UMLs/carbonatites, and members of the Cretaceous nephelinite suite from the Aillik Bay area. (A) For the lamproite source region, a Pb–Pb evolution of initial $\mu_1 \sim 8$ until 2.3 Ga and subsequent evolution in a second-stage low μ environment at $\mu_2 \sim 4.5$ is suggested by the measured and initial lamproite Pb isotope composition. (B) Enlarged portion of Pb–Pb isotope space with model two-stage Pb–Pb evolution lines for the nephelinite source region assuming an initial μ_1 value of ~8.2 from 4.55 Ga until 0.7 Ga and 1.1 Ga, respectively, and subsequent evolution with second-stage μ_2 values of 25 and 30, respectively. Tick marks on evolution lines indicate time steps of 100 Myr. The 'Stacey and Kramers' Pb evolution curve (S & K, [80]) is shown for reference with tick marks for 250 Myr intervals. The relatively large error envelopes indicate typical 2σ errors for the UML suite (whiskers in A; error ellipse in B) due to the combined effects of uncertainties from the high measured U/Pb ratios and large age corrections. The cumulative 2σ errors for the lamproites and nephelinites are smaller than symbol size. Ancient enriched Laurentia SCLM as defined by potassic anorogenic magma compositions and micaceous SCLM xenoliths: [39,57–62]. Primitive Cretaceous alkali basalts from the nearby New England Seamount Chain [67] are shown for comparison. Modern MORB and OIB data were compiled by A. Stracke from literature and database sources. The position of the present-day geochron was calculated assuming an age of the Earth of 4.55 Ga and initial Pb isotope composition similar to the Canyon Diablo troilite.

isotope compositional range of the nephelinite suite (Figs. 5, 6 and 7).

5. Discussion

5.1. Depths of magma origin

The deep lithosphere structure of the NAC is poorly understood compared to the Kaapvaal, Siberian, and Slave cratons. Studies on mantle-derived xenoliths are sparse and so far restricted to the Greenland portion of the NAC [40–42]. However, a combination of thermobarometry on peridotitic lithologies and major and trace element compositions indicate a general increase in fertility and a stronger metasomatic imprint towards the base of the subcontinental lithospheric mantle (SCLM). The deepest conditions recorded by garnet peridotites from West Greenland scatter around 6.3 GPa and 1270–1300 °C at the eruption age of ca. 600 Ma [40]. These high pressure samples (>5 GPa) define conductive geotherms slightly above 40 mWm^{-2} [40,41] and their aillikite host rocks contain diamonds, consistent with the presence of a deep lithospheric mantle root at this time.

Results from experimental petrology provide robust information on the depth of final melt segregation. Experiments on an olivine lamproite composition by Foley [43] demonstrated that multiple saturation of a mica harzburgite mineralogy occurred under the presence of reduced C–O–H fluids ($H_2O > CH_4$) at pressures in excess of 5 GPa. This is consistent with diamond discoveries in olivine lamproites from Western Australia and India. For the aillikites, the simple CMAS–CO_2 system melting experiments by [44] and [45] are the most appropriate available. These experiments showed that transitional carbonate–ultramafic silicate magmas similar to aillikites can form from carbonated peridotite over a pressure interval between 4 and 7 GPa, which is in keeping with the occurrence of diamonds in numerous aillikite dykes in the North Atlantic region [19,36]. Earlier experiments had shown that silica-poor mafic alkaline compositions such as melilitites, nephelinites, and basanites may form as low-degree melts from peridotite in the presence of H_2O and CO_2 at 2.5 to 3.5 GPa [46–49]. The most Si-deficient composition of the Aillik Bay nephelinite suite is the olivine melilitite ST103 (SiO_2 < 35 wt.%), which resembles the Sutherland olivine melilitites of South Africa for which four-phase peridotite saturation was achieved between 3 and 3.5 GPa under high CO_2 pressures [50]. According to these experiments, 3.5 GPa would be the maximum pressure of melt segregation for the Aillik Bay nephelinite suite. The observed intra-suite compositional range towards basanite may be explained by slightly higher degrees of melting due to increasing temperature and/or increasing H_2O/CO_2 ratios [47]. Alternatively, polybaric melting within a 3.5 to 2.5 GPa pressure range may alone account for the spectrum of sodic mafic alkaline magmas.

The experimental studies outlined above indicate that the olivine lamproites and aillikites from the Labrador Sea margins could have formed under similarly high pressures well within the diamond stability field (>4.5 GPa), whereas a significant shallowing of the melting process (2.5–3.5 GPa) is required for the genesis of the younger Cretaceous nephelinites. However, all three alkaline magma types require hydrous minerals in the upper mantle source assemblages, with phlogopite and amphibole being considered most important (e.g., [43,51–53]). Therefore, the melts must have equilibrated in relatively cold mantle lithosphere owing to the restricted thermal stability of hydrous minerals. With this in mind, the isotopic data of primitive olivine lamproites (1374 Ma), aillikites/carbonatites (590–555 Ma), and nephelinites (142 Ma) from the Aillik Bay area may provide information about the transient geochemical and geothermal evolution of the mantle at the base of the NAC lithosphere.

5.2. Alkaline magma source regions through time

The initial Pb isotope composition of the Mesoproterozoic lamproites falls significantly to the left of the geochron along an upper mantle Pb growth curve defined by a μ-value of ~8 (Fig. 7). The least radiogenic initial Pb lies close to the intersection between this mantle evolution curve and a 2.3 Ga isochron. Lamproite Pb is thus considerably less radiogenic than Pb within the convective Earth mantle at the time of melt extraction at 1.37 Ga. The simplest explanation would be Pb withdrawal from the convective mantle (μ_1 of ~8) during the Paleoproterozoic (~2.3 Ga) and further isolated evolution of this Pb in a low U/Pb environment with a second-stage μ_2 of about 4 to 5 until lamproite melt extraction at 1.37 Ga (measured $\mu = 4.5 \pm 2.3$). This extraordinarily unradiogenic Pb isotope composition suggests that the pronounced U depletion (Fig. 4) is a primary source feature, which is also recognized in other Laurentian lamproites such as the time equivalents from Sisimiut, and the Miocene Smoky Butte madupites [39,54]. However, the LREE and majority of HFSE must have been strongly enriched within this isolated mantle reservoir by about the same time the U depletion occurred, as evident from the highly unradiogenic initial Nd (low Sm/Nd) and Hf (low Lu/Hf) isotope compositions (Fig. 6) and the consistently old Nd and Hf depleted mantle model ages (2.1–2.4 Ga; Table 2). Such low time-

integrated Lu/Hf, required to maintain the unradiogenic $^{176}Hf/^{177}Hf$ of the lamproite source region, is typically found in garnet-poor pyroxenitic lithologies [55], but not in garnet peridotites, even if the latter show clear enrichment in terms of their Sr and Nd isotope compositions [56].

The moderately radiogenic initial $^{87}Sr/^{86}Sr$ (<0.7062) indicates that fairly low time-integrated Rb/Sr was coupled to the strong LREE enrichment of the lamproite source region. This suggests that K-metasomatism (i.e., phlogopitization) occurred shortly prior to lamproite magmatism. Alternatively, the involvement of a subordinate CO_2-component could account for this apparent Sr–Nd isotope decoupling; such a proposal was made by Nelson [39] in order to explain the unusual Sr–Nd isotopic composition of the 'enriched mantle' type involved in the genesis of many Laurentian lamproites (Fig. 5). Although this hypothesis contradicts the absence of carbonate in archetypal Wyoming craton lamproites from Leucite Hills and Smoky Butte [36,54], the presence of CO_2 metasomatites in the NAC lamproite mantle reservoir is supported by the ubiquitous but small amounts of interstitial carbonate in the Aillik Bay lamproites, as also reported from their Sisimiut and Napoleon Bay analogues. Aillik Bay lamproite carbonate has $\delta^{13}C$ compositions between −6.4 and −5.5‰ testifying to a primary mantle origin (Supplementary file D).

In short, the source region of the Aillik Bay olivine lamproites was compositionally heterogeneous with a complex geochemical evolution as part of the lowermost SCLM. Clinopyroxene-rich lithologies have almost certainly been involved in lamproite genesis, presumably as veins within peridotite representing convective mantle-derived fluids/melts that had been injected into the SCLM during the Paleoproterozoic (2.4–2.1 Ga). Phlogopite formation in the lamproite source occurred at a later stage but appears to be unrelated to subduction zone processes that led to the incorporation of the NAC into the Laurentia assembly at ca. 1.9–1.7 Ga as typical convergent margin magma trace element signatures such as Nb–Ta–Ti depletions are lacking.

In contrast, the Neoproterozoic aillikites have juvenile initial Pb isotope compositions close to the geochron although the compositional range extends from radiogenic values typical for convective mantle material (i.e., depleted MORB mantle) towards unradiogenic values slightly to the left of the geochron (Fig. 7). This unradiogenic end-member in a $^{206}Pb/^{204}Pb$ vs $^{207}Pb/^{204}Pb$ diagram straddles the compositional field for ancient enriched Laurentia SCLM as compiled from North American ultrapotassic magmas and their micaceous mantle xenoliths (e.g., [39,57–62]). Fairly juvenile isotope signatures are apparent from the slightly positive $\varepsilon_{Nd(i)}$ and $\varepsilon_{Hf(i)}$ values close to CHUR (Fig. 6). However, calculated Nd and Hf depleted mantle model ages range between 1.2 and 1.0 Ga (Table 2), thus indicating that an older component must have been involved during aillikite magma production, as is also evident from Pb isotope compositions falling partly to the left of the geochron.

Tappe et al. [10] favoured a genetic model for aillikite magma production that invokes the remelting of young carbonate–phlogopite veins in garnet peridotite at the base of the cratonic SCLM. This mechanism can account for both the thermal stability of the required hydrous source mineralogy and the juvenile radiogenic isotope signature of aillikites since the carbonate veins originate as low-degree melts of the convective mantle shortly beforehand. Their remelting causes extensive volatile-fluxed melting of the surrounding peridotite [63] so that the incompatible trace element budget, and in turn Sr, Nd, and Hf isotope signature, of a carbonate-silicate magma blend is controlled by the convective mantle-derived carbonate vein component. However, an important inference from the previous alkaline magmatism of the deep NAC lithosphere is the likelihood of subordinate long-term enriched phlogopite–clinopyroxene material left after the 1.37 Ga lamproite melting event. Carbonate-fluxed melting almost certainly remobilized the isotopically extreme components together with surrounding garnet peridotite so that a mildly depleted isotope signature of invading carbonate-rich magmas is shifted slightly towards more 'enriched' values. The isotope data suggest that the impact of such ancient enriched SCLM material on convective mantle-derived carbonate melts is strongest with respect to Pb isotopes (Fig. 7), because residual phlogopite can store significant amounts of Pb in the cratonic mantle [64] and is consumed during subsequent partial melting events.

Simple binary mixing calculations between mildly depleted convective mantle (e.g., 75% Depleted Mantle plus 25% Primitive Mantle) and long-term enriched SCLM isotope end-members yielded the observed aillikite Sr–Nd–Hf isotope compositions when 20 to 40% of incompatible element rich carbonate vein melts derived from the convecting mantle (Sr=5500 ppm; Nd=350 ppm; Hf=40 ppm; $^{87}Sr/^{86}Sr_{(582)}=0.702589$; $^{143}Nd/^{144}Nd_{(582)}=0.51207$; $^{176}Hf/^{177}Hf_{(582)}=0.28261$) blend with MgO-rich, higher degree melts of enriched SCLM garnet peridotite (Sr=480 ppm; Nd=25.3 ppm; Hf=2.1 ppm). Old phlogopite–clinopyroxenes are envisaged as forming part of the deep SCLM and melts of such exotic materials dominate the Sr–Nd–Hf element budget of any hybrid wall-

rock component. Thus, the inferred isotope composition of the lamproite source (time integrated to 582 Ma) is assigned as the long-term enriched end-member ($^{87}Sr/^{86}Sr_{(582)}$=0.707931; $^{143}Nd/^{144}Nd_{(582)}$= 0.511103; $^{176}Hf/^{177}Hf_{(582)}$=0.281734; Figs. 5 and 6).

The carbonate melt introduction into the SCLM (veining) must have occurred shortly prior to aillikite melt segregation, because the Nd and Hf isotope systems are strongly coupled, with aillikites falling on the terrestrial array [65]. Bizimis et al. [66] demonstrated that mantle carbonate assemblages are capable of producing anomalously radiogenic Hf on a short timescale (10–50 Myr) due to their extremely high Lu/Hf, while leaving the Nd isotopes unaffected. Hence, melting of aged mantle carbonate would result in a significant departure from the terrestrial Nd–Hf isotope array along a vertical trend whose vector can be inferred from the analyzed Aillik Bay carbonatites (although they are still within the array due to the young age of the carbonate infiltration; Fig. 6). Following this argument, the Nd and Hf depleted mantle model ages of the aillikites, which precede Neoproterozoic magmatism by at least 400 Myr (taking melting-related parent/daughter element fractionation into account), form a mixture of a long-term enriched SCLM component that was melted together with the juvenile carbonate material.

The Cretaceous nephelinite suite shows rather unusual isotope signatures. For example, the highly radiogenic Pb isotope data imply the involvement of convective mantle material similar to components that contributed to the Cretaceous alkali basalts of the New England Seamounts in the North Atlantic (Fig. 7; [67]). In contrast, the negative $\varepsilon_{Nd(i)}$ values and radiogenic Sr isotope compositions, which differ from more 'depleted' values for these seamounts, point to melt contribution from a long-term enriched reservoir (Fig. 5), and a juvenile isotope signature is apparent from the initial Hf isotope data close to Bulk Earth (Fig. 6). Such deviations from modern oceanic Sr–Nd–Hf–Pb isotope systematics are most likely produced within SCLM over geological time. However, the deep long-term enriched SCLM that was tracked by the Mesoproterozoic lamproites is not an appropriate source region for the Cretaceous nephelinites, because its extremely unradiogenic Pb isotope composition would impart a detectable low-$^{207}Pb/^{204}Pb$ imprint on the nephelinitic melts, which is not observed. Furthermore, the Nd and Hf depleted mantle model ages for the nephelinite suite indicate Neoproterozoic source enrichment (0.7–1.1 Ga), as opposed to the Paleoproterozoic model ages derived from the lamproites.

The metasomatism of the source region of the nephelinites was probably related to the aillikite magmatism some 500 Myr earlier. Moore and Wood [68] demonstrated experimentally that carbonate-rich magmas such as aillikites would react with peridotites, releasing CO_2 and causing the formation of clinopyroxene-rich assemblages ('wehrlitization'). The pressure of origin of the nephelinite suite is particularly prone to this type of decarbonation reaction due to a prominent ledge in the peridotite solidus (Fig. 8). It is therefore reasonable to assume that before the first aillikite magma reached the surface in the Aillik Bay area at ca. 590 Ma, appreciable volumes of the shallower SCLM (ca. 2.5–3.0 GPa) had been metasomatically converted by passing carbonate-rich magmas. This metasomatized region within the shallow SCLM appears to have produced the Cretaceous nephelinitic magmas with their characteristically high CaO/Al_2O_3 at ca. 142 Ma after a drastic change in the thermal structure of the cratonic lithosphere had occurred.

Strong support for a carbonate metasomatic imprint on the shallower SCLM comes from the incompatible element distribution of the nephelinite suite resembling that of the aillikites (Fig. 4), which may serve as a proxy for the metasomatic agent. Since newly grown clinopyroxene, pargasitic amphibole, and/or phlogopite (see order of magnitude Cs variation of nephelinites) largely control the incompatible trace element budget of cratonic peridotites in the shallow upper mantle, they are capable of leaving a fingerprint from the inherited metasomatic component on the newly derived melt; for example, the suprachondritic Zr/Hf of the Aillik Bay nephelinite suite strongly points to a 'carbonate-rich' metasomatic agent [69]. Furthermore, isotopic evolution of this metasomatic component in isolation from mantle convection for some 500 Myr could account for the observed unusual isotope features of the Cretaceous nephelinite suite. Thus, we favour the following explanation:

(1) Negative $\varepsilon_{Nd(i)}$ values are due to retarded radiogenic in-growth in the metasomatically altered part of the shallow SCLM as a function of extremely low Sm/Nd of the carbonate–silicate metasomatic agent (0.10±0.01 for aillikites; as compared to 0.20 for CHUR). (2) Bulk Earth-like $\varepsilon_{Hf(i)}$ values similar to aillikites (Fig. 6) are due to near chondritic Lu/Hf of the carbonate–silicate metasomatic agent (0.02±0.01 for aillikites; as compared to 0.03 for CHUR). (3) Highly radiogenic $^{206}Pb/^{204}Pb_{(i)}$ isotope compositions are due to enhanced radiogenic in-growth ($\mu_2 \sim 25$–30) caused by elevated U/Pb of the carbonate–silicate metasomatic agent (i.e., aillikites have average μ-values of 25.4±10), subsequent to a normal mantle evolution ($\mu_1 \sim 8.2$; Fig. 7B).

5.3. Deep mantle melting during temporal rift evolution

The observation that lamproite, aillikite/carbonatite, and nephelinite magmas were produced at the base of a single cratonic block over 1200 Myr is best explained by variation in the SCLM thickness with time, coupled with distinctive metasomatic overprinting, both of which are linked to past magmatic and tectonic events (Fig. 9). The hydrous-dominated nature of the lamproites and the occurrence of subordinate primary carbonate indicate melting under oxygen fugacity conditions close to the H_2O-maximum defined by C–H_2O [70], corresponding to IW+2 log units (< FMQ), where small amounts of CO_3^{2-} can be dissolved in a H_2O-rich silicate melt. However, melting of cold cratonic SCLM (~35–40 mWm^{-2}) is difficult even under H_2O-bearing conditions. It appears that only at the craton margins and in surrounding mobile belts, where heat is diverted away from the stiff craton interior [2], local deflections of the conductive geotherm may intersect with rather reduced lithosphere solidi (Fig. 8A). This may help to explain the rarity of olivine lamproites and their preferred affiliation to circum-cratonic settings in areas without thermal anomalies [54].

Although this cratonic SCLM appears to have been largely intact during the Mesoproterozoic forming part of the young stagnant Laurentia supercontinent [23], there is evidence for early interaction with upwelling asthenosphere at the southern NAC edge. The mantle underneath the Gardar region in SW Greenland (Fig. 1) produced UMLs and carbonatites between ca. 1300–1160 Ma [26], indicating the presence of locally thinned and oxidized NAC lithosphere during the Mesoproterozoic. The Aillik Bay lamproites predate "Gardar rifting" by about 100 Myr (Fig. 2) and appear to have formed during a more immature stage of this prolonged SCLM conversion, with melting taking place exclusively within deep long-term enriched and slightly reduced SCLM.

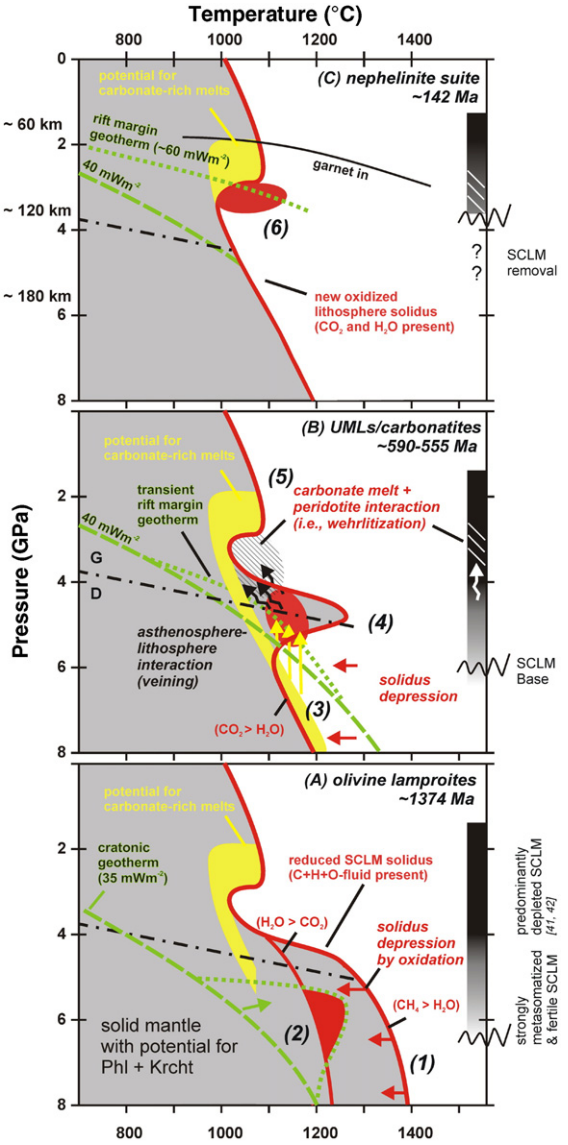

Fig. 8. Pressure–temperature diagram to illustrate deep alkaline magma production during temporal evolution of a rift cutting through cratonic lithosphere. (A) Mesoproterozoic olivine lamproites form after the pyrolite dehydration solidus has been depressed *(1)* by beginning oxidation of convective mantle-derived volatiles and thermal perturbations at the craton margin that locally deflect the geotherm *(2)* thereby facilitating intersection with the solidus. (B) Extension of the SCLM during the Neoproterozoic causes progressive oxidation of ascending C–H–O fluids so that CO_2 becomes the predominant volatile-species *(3)* at the boundary between lithosphere and asthenosphere. Low-degree convective mantle-derived melts form under cratonic conditions and freeze at the base of the relatively cold SCLM forming carbonate-rich veins. As stretching continues, the SCLM starts to heat and newly adjusted warmer geotherms enable remelting of carbonate veins plus peridotite/pyroxenite wall-rock *(4)*. The produced transitional carbonate–silicate magmas such as aillikites are prone to undergo decarbonation reactions with peridotite during their ascent at pressures of about 2.5–3.0 GPa *(5)*. This particular region of the shallower SCLM is therefore expected to have been converted into clinopyroxene-rich and ± pargasite- and phlogopite-bearing peridotitic lithologies. (C) Extensive Mesozoic stretching of the SCLM established a depressed oxidized pyrolite dehydration solidus and a warm rift-margin geotherm so that production of mafic alkaline melts was facilitated at much shallower depths than previous aillikite generation within the region where Neoproterozoic carbonate metasomatism had occurred *(6)*. This petrogenetic model along with the geochemical information obtained during this study suggests that at least 30 km of cratonic SCLM must have been convectively removed between ca. 550 Ma and 150 Ma. Solidi of pyrolitic mantle for reduced H_2O-undersaturated (dehydration solidus, C+H-fluid present) and oxidized CO_2-bearing conditions, as well as 'garnet in' curve are taken from [49]. References for geotherms and graphite (G) – diamond (D) stability curve can be found in the caption to Figure 21 of [10].

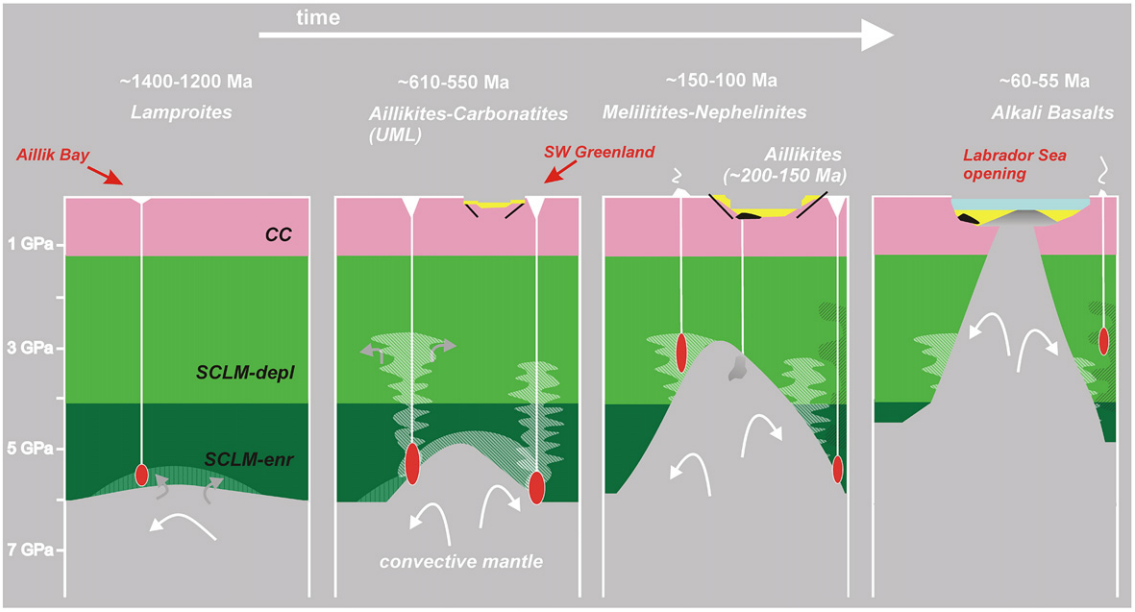

Fig. 9. Tectonomagmatic model for a segment of the NAC close to the southern craton margin. Mesoproterozoic lamproite melting occurred at the base of long-term enriched SCLM (vertically hatched pattern), whereas Neoproterozoic aillikites formed during extensive interaction between this ancient SCLM and the upwelling asthenosphere. In contrast, the Cretaceous nephelinite suite was produced within a shallower SCLM region that had experienced carbonate metasomatism during the >30 Myr of Neoproterozoic aillikite/carbonatite magmatism (diagonally hatched pattern). Heat for partial melting (new rift margin geotherm) was provided by the upwelling convective mantle, which appears to have delaminated deeper parts of the previously fluid and melt infiltrated NAC lithosphere. Typical continental rift development with prominent surface expressions such as graben structures occurred during the Early Cretaceous (ca. 140 Ma) after several kilometres of the cratonic SCLM had been convectively removed. The final break-up of the NAC occurred at ca. 60 Ma with the initiation of sea-floor spreading in the Labrador Sea.

Neoproterozoic aillikite magma production was more widespread than lamproite magmatism, affecting both the on-craton and circum-cratonic portions of the NAC (Fig. 1), which points to intensified lithosphere stretching contemporaneous with rifting in the nearby Iapetus Ocean basin [71]. Moreover, the proximity of aillikite intrusives to the present-day Labrador Sea margins suggests a pronounced structural control of melt production by thermo-tectonic processes in the vicinity of this lithospheric discontinuity. The fairly juvenile Sr–Nd–Hf–Pb isotope compositions of UMLs/carbonatites (Figs. 5–7) indicate regional protrusion of asthenosphere into the overlying cratonic SCLM along active Late Neoproterozoic deep fracture zones. Convective mantle-derived C–H–O fluids depressed the solidus by several hundred degrees [70,72] until CO_2 eventually became the dominant volatile species (aillikite olivine-spinel pairs record oxidized fO_2 > FMQ, [10]) resulting in CO_2-rich low-degree melts under both cratonic and circum-cratonic conditions (40–50 mWm^{-2}) at a newly adjusting asthenosphere–lithosphere boundary (Fig. 8B). Since these carbonate melts have a very low heat capacity [73] they freeze as soon as they encounter colder regions of the upward and outward moved cratonic base ('veining'). A sequence of complex melting processes during subsequent lithosphere–asthenosphere interactions is supported by the fact that UML/carbonatite magmatism prevailed for over 30 Myr in the Aillik Bay area and was relatively voluminous for a magma type considered to be a "low-degree" melt. However, a progressive change from cratonic to rift margin-like geotherms during this prolonged 'failed' rifting attempt was crucial to aillikite genesis (Fig. 8B).

The Late Mesozoic–Cenozoic rifting episode of the NAC was more intense than the previous ones, resulting in the opening of an ocean basin [74]. However, the earliest extension stages (ca. 200–150 Ma; Fig. 2) produced deep aillikite and carbonatite magmas beneath the craton interior [17,27–29,75], which are petrologically very similar to their Neoproterozoic counterparts [36]. At about 150 Ma, a marked switch from the production of potassic–carbonatitic to sodic alkaline magma types occurred (Fig. 2). This coincides with the onset of rift basin formation along the present-day Labrador Sea margins with Early Cretaceous terrigenous sediments representing the oldest sedimentary record on both the Labrador and Greenland shelves [16,25]. The convective mantle had reached shallow

levels along the rift axis during the Early Cretaceous (Fig. 9) as demonstrated by model calculations for the Alexis Formation alkaline basaltic flows (ca. 140–120 Ma) located ca. 200 km off-shore central Labrador [76]. This modelling suggests stretching and thinning of the lithosphere along the rift axis atop small-scale convection cells with higher than 'normal' potential temperatures of 1400 °C in order to account for the observed basalt volumes. The more distant areas to the developing rift depression, such as Aillik Bay, must have experienced a shift towards 'warmer' conductive geotherms but presumably not exceeding 60 mWm^{-2}. Under these rift margin conditions, small volumes of mafic alkaline magma were produced at much shallower depths than previous aillikite magmatism, because an elevated geotherm could intersect with a depressed, H_2O- and CO_2- present peridotite solidus at relatively shallow SCLM levels (Fig. 8C).

6. Implications for craton reactivation

The observed sequence of deep melting processes beneath Aillik Bay is representative for the 'younger' alkaline magmatic history of the NAC (Fig. 9) and has wider implications for the reactivation of cratonic lithosphere. While a deep and long-term enriched cratonic base (>150 km depth) was present throughout the Proterozoic and served as a magma source for ultrapotassic lamproites and in part for potassic–carbonatitic aillikites, it seems to have been lost shortly prior to Cretaceous rifting (Fig. 9). If 4.5 GPa is considered the minimum pressure under which aillikite magma segregation occurred during the Neoproterozoic, and 3.5 GPa the maximum pressure of melting to generate the Cretaceous nephelinite suite, then the asthenosphere–lithosphere boundary beneath Aillik Bay must have moved at least 30 km upwards between 550 Ma and 150 Ma. Unfortunately, this cannot be resolved any better for the craton margin beneath Aillik Bay, but it is interesting to note that Jurassic aillikite magmatism in West Greenland occurred exclusively in the interior parts of the now split craton, but not at the margins and surrounding mobile belts. It therefore appears that a deep cratonic root had survived convective mantle-derived stresses beneath the craton interior until the Jurassic but was removed shortly prior to the Early Cretaceous continental rift basin formation. It is reasonable to speculate that the integrity of the cratonic mantle had been significantly modified by regionally widespread and recurrent carbonatite magmatism so that the deep parts of the cratonic lithosphere could be effectively removed by stretching and thinning during plate tectonic stresses (Fig. 9). Our conservative estimate of ~30 km cratonic mantle lithosphere removal beneath the southern NAC margin occurred prior to a 'normal' continental rift development with marked surface expressions such as rifted sedimentary basins as typically developed on Phanerozoic platforms with an average lithospheric thickness of about 100 km. This furthermore implies that the earliest rifting of cratonic lithosphere is confined to its deepest parts, with fluid and melt ingress from below playing an important role in chemically converting SCLM and thereby creating zones of persistent lithospheric weakness.

Acknowledgments

George Jenner is thanked for the support in the preparatory stages of this study, which was conducted within the DFG projects Fo 181/15 and STR 853/2 (Germany). ST acknowledges a Max-Planck Society post doctoral fellowship and invitation to fieldwork in Greenland in 2006 by the Geological Survey of Denmark and Greenland, where many of the arguments presented herein had been shaped. Financial support from IAVCEI for the attendance of ST to the General Assembly 2006 in China is gratefully acknowledged. The manuscript benefited from constructive and refreshingly open-minded comments by Graham Pearson and an anonymous reviewer, for which we are sincerely grateful. We are furthermore indebted to Lotte Larsen, Dejan Prelevic, Zoran Jovanovic, and Mike Villeneuve for informal reviews and helpful discussions that ensued during data presentation. This is Geological Survey of Canada Contribution 20060538.

Appendix A. Supplementary data

Supplementary data associated with this article can be found, in the online version, at doi:10.1016/j.epsl.2007.01.036.

References

[1] T.H. Jordan, Composition and development of the continental tectosphere, Nature 274 (1978) 544–548.
[2] H.N. Pollack, Cratonization and thermal evolution of the mantle, Earth Planet. Sci. Lett. 80 (1986) 175–182.
[3] D.G. Pearson, R.W. Carlson, S.B. Shirey, F.R. Boyd, P.H. Nixon, Stabilisation of Archaean lithospheric mantle: a Re–Os isotope study of peridotite xenoliths from the Kaapvaal Craton, Earth Planet. Sci. Lett. 134 (1995) 341–357.
[4] W.L. Griffin, S.Y. O'Reilly, N. Abe, S. Aulbach, R.M. Davies, N.J. Pearson, B.J. Doyle, K. Kivi, The origin and evolution of Archean lithospheric mantle, Precambrian Res. 127 (2003) 19–41.
[5] S.D. King, Archean cratons and mantle dynamics, Earth Planet. Sci. Lett. 234 (2005) 1–14.

[6] M.A. Menzies, W.M. Fan, M. Zhang, Palaeozoic and Cenozoic lithoprobes and the loss of >120 km of Archaean lithosphere, Sino-Korean craton, China, in: H.M. Prichard, T. Alabaster, N.B.W. Harris, C.R. Neary (Eds.), Magmatic Processes and Plate Tectonics, vol. 76, Geological Society of London, London, UK, 1993, pp. 71–81.
[7] C. Ebinger, Y.P. Djomani, E. Mbede, A. Foster, J.B. Dawson, Rifting Archaean lithosphere: the Eyasi–Manyara–Natron rifts, East Africa, J. Geol. Soc. 154 (1997) 947–960.
[8] D.E. Jacob, K.S. Viljoen, N. Grassineau, E. Jagoutz, Remobilization in the cratonic lithosphere recorded in polycrystalline diamond, Science 289 (2000) 1182–1185.
[9] S.F. Foley, A.V. Andronikov, D.E. Jacob, S. Melzer, Evidence from Antarctic mantle peridotite xenoliths for changes in mineralogy, geochemistry and geothermal gradients beneath a developing rift, Geochim. Cosmochim. Acta 70 (2006) 3096–3120.
[10] S. Tappe, S.F. Foley, G.A. Jenner, L.M. Heaman, B.A. Kjarsgaard, R.L. Romer, A. Stracke, N. Joyce, J. Hoefs, Genesis of ultramafic lamprophyres and carbonatites at Aillik Bay, Labrador: a consequence of incipient lithospheric thinning beneath the North Atlantic craton, J. Petrol. 47 (2006) 1261–1315.
[11] W.M. Fan, H.F. Zhang, J.A. Baker, K.E. Jarvis, P.R.D. Mason, M.A. Menzies, On and off the North China Craton: where is the Archaean keel? J. Petrol. 41 (2000) 933–950.
[12] S. Gao, R.L. Rudnick, R.W. Carlson, W.F. McDonough, Y. Liu, Re–Os evidence for replacement of ancient mantle lithosphere beneath the North China Craton, Earth Planet. Sci. Lett. 198 (2002) 307–322.
[13] D. Bridgwater, J. Watson, B.F. Windley, The Archaean craton of the North Atlantic region, Philos. Trans. R. Soc. Lond. 273 (1973) 493–512.
[14] A.P. Nutman, K.D. Collerson, Very early Archean crustal-accretion complexes preserved in the North Atlantic Craton, Geology 19 (1991) 791–794.
[15] D. Chian, K.E. Louden, C.E. Keen, I. Reid, Evolution of nonvolcanic rifted margins: new results from the conjugate margins of the Labrador Sea, Geology 23 (1995) 589–592.
[16] J.A. Chalmers, T.C.R. Pulvertaft, Development of the continental margins of the Labrador Sea: a review, in: R.C.L. Wilson, R.B. Whitmarsh, B. Taylor, N. Froitzheim (Eds.), Non-Volcanic Rifting of Continental Margins: A Comparison of Evidence from Land and Sea, vol. 187, Geological Society of London, London, UK, 2001, pp. 77–105.
[17] L.M. Larsen, D.C. Rex, A review of the 2500 Ma span of alkaline-ultramafic, potassic and carbonatitic magmatism in West Greenland, Lithos 28 (1992) 367–402.
[18] D.D. Hogarth, Mineralogy of leucite-bearing dykes from Napoleon Bay, Baffin Island: multistage Proterozoic lamproites, Can. Mineral. 35 (1997) 53–78.
[19] S. Digonnet, N. Goulet, J. Bourne, R. Stevenson, D. Archibald, Petrology of the Abloviak aillikite dykes, New Québec: evidence for a Cambrian diamondiferous alkaline province in northeastern North America, Can. J. Earth Sci. 37 (2000) 517–533.
[20] S. Tappe, G.A. Jenner, S.F. Foley, L.M. Heaman, D. Besserer, B.A. Kjarsgaard, A.B. Ryan, Torngat ultramafic lamprophyres and their relation to the North Atlantic Alkaline Province, Lithos 76 (2004) 491–518.
[21] S. Tappe, S.F. Foley, B.A. Kjarsgaard, L.M. Heaman, G.A. Jenner, A. Stracke, R.L. Romer, Ultramafic lamprophyres and carbonatites of Labrador and New Quebec: towards a genetic model for Neoproterozoic rift-related alkaline magmatism in the North Atlantic region, Rep. — Geol. Surv. Den. Greenl. 68 (2005) 115–117.
[22] L. Schiøtte, B.T. Hansen, S.B. Shirey, D. Bridgwater, Petrological and whole rock isotopic characteristics of tectonically juxtaposed Archaean gneisses in the Okak area of the Nain Province, Labrador: relevance for terrane models, Precambrian Res. 63 (1993) 293–323.
[23] P.F. Hoffman, Speculations on Laurentia's first gigayear (2.0 to 1.0 Ga), Geology 17 (1989) 135–138.
[24] R.J. Wardle, J. Hall, Proterozoic evolution of the northeastern Canadian Shield: Lithoprobe Eastern Canadian Shield Onshore–Offshore Transect (ECSOOT), introduction and summary, Can. J. Earth Sci. 39 (2002) 563–567.
[25] H.R. Balkwill, N.J. McMillan, B. Maclean, G.L. Williams, S.P. Srivastava, Geology of the Labrador Shelf, Baffin Bay, and Davis Strait, in: M.J. Keen, G.L. Williams (Eds.), Geology of the Continental Margin of Eastern Canada Geology of Canada, vol. 2, Geological Survey of Canada, Ottawa, 1990, pp. 293–348.
[26] B.G.J. Upton, C.H. Emeleus, L.M. Heaman, K.M. Goodenough, A.A. Finch, Magmatism of the mid-Proterozoic Gardar Province, South Greenland: chronology, petrogenesis and geological setting, Lithos 68 (2003) 43–65.
[27] M. Bizzarro, A. Simonetti, R.K. Stevenson, J. David, Hf isotope evidence for a hidden mantle reservoir, Geology 30 (2002) 771–774.
[28] L.M. Larsen, Mesozoic to Palaeogene dyke swarms in West Greenland and their significance for the formation of the Labrador Sea and the Davis Strait, Rep. — Geol. Surv. Den. Greenl. 2006/34 (2006) 1–69.
[29] A. Steenfelt, J.A. Hollis, K. Secher, The Tikiusaaq carbonatite: a new Mesozoic intrusive complex in southern West Greenland? Geol. Surv. Den. Greenl. Bull. 7 (2006) 9–12.
[30] B.H. Scott, Kimberlite and lamproite dykes from Holsteinsborg, West Greenland, Meddelelser om Grønland, Geoscience 4 (1981) 3–24.
[31] L.M. Heaman, Patterns of kimberlite emplacement: the importance of robust geochronology, Rep. — Geol. Surv. Den. Greenl. 68 (2005) 25.
[32] D.C. Umpleby, Geology of the Labrador Shelf, Rep. Geol. Surv. Can. 79/13 (1979) 1–34.
[33] A.F. King, N.J. McMillan, A Mid-Mesozoic breccia from the coast of Labrador, Can. J. Earth Sci. 12 (1975) 44–51.
[34] L.M. Larsen, D.C. Rex, W.S. Watt, P.G. Guise, $^{40}Ar/^{39}Ar$ dating of alkali basaltic dykes along the southwest coast of Greenland: Cretaceous and Tertiary igneous activity along the eastern margin of the Labrador Sea, Geol. Greenl. Surv. Bull. 184 (1999) 19–29.
[35] K. Hansen, Lamprophyres and carbonatitic lamprophyres related to rifting in the Labrador Sea, Lithos 13 (1980) 145–152.
[36] S. Tappe, S.F. Foley, G.A. Jenner, B.A. Kjarsgaard, Integrating ultramafic lamprophyres into the IUGS classification of igneous rocks: rational and implications, J. Petrol. 46 (2005) 1893–1900.
[37] R.H. Mitchell, Carbonatites and carbonatites and carbonatites, Can. Mineral. 43 (2005) 2049–2068.
[38] H. Palme, H.S.C. O'Neill, Cosmochemical estimates of mantle composition, in: R.W. Carlson (Ed.), Treatise on Geochemistry, vol. 2, Elsevier, Amsterdam, 2003, pp. 1–38.
[39] D.R. Nelson, Isotopic characteristics and petrogenesis of the lamproites and kimberlites of central West Greenland, Lithos 22 (1989) 265–274.
[40] M. Bizzarro, R. Stevenson, Major element composition of the lithospheric mantle under the North Atlantic craton: evidence from peridotite xenoliths of the Sarfartoq area, southwestern Greenland, Contrib. Mineral. Petrol. 146 (2003) 223–240.

[41] W.L. Griffin, S.Y. O'Reilly, B.J. Doyle, N.J. Pearson, H. Coopersmith, K. Kivi, V.G. Malkovets, N.P. Pokhilenko, Lithosphere mapping beneath the North American plate, Lithos 77 (2004) 873–922.
[42] S. Bernstein, K. Hanghøj, P.B. Kelemen, C.K. Brooks, Ultra-depleted, shallow cratonic mantle beneath West Greenland: dunitic xenoliths from Ubekendt Ejland, Contrib. Mineral. Petrol. 152 (2006) 335–347.
[43] S.F. Foley, An experimental study of olivine lamproite: first results from the diamond stability field, Geochim. Cosmochim. Acta 57 (1993) 483–489.
[44] J.A. Dalton, D.C. Presnall, The continuum of primary carbonatitic–kimberlitic melt compositions in equilibrium with lherzolite: data from the system $CaO–MgO–Al_2O_3–SiO_2–CO_2$ at 6 GPa, J. Petrol. 39 (1998) 1953–1964.
[45] G.H. Gudfinnsson, D.C. Presnall, Continuous gradations among primary carbonatitic, kimberlitic, melilititic, basaltic, picritic, and komatiitic melts in equilibrium with garnet lherzolite at 3–8 GPa, J. Petrol. 46 (2005) 1645–1659.
[46] D.H. Green, Conditions of melting of basanite magma from garnet peridotite, Earth Planet. Sci. Lett. 17 (1973) 456–465.
[47] G. Brey, D.H. Green, Systematic study of liquidus phase relations in olivine melilitite $+H_2O+CO_2$ at high pressures and petrogenesis of an olivine melilitite magma, Contrib. Mineral. Petrol. 61 (1977) 141–162.
[48] K. Hirose, Partial melt compositions of carbonated peridotite at 3 GPa and role of CO_2 in alkali-basalt magma generation, Geophys. Res. Lett. 24 (1997) 2837–2840.
[49] D.H. Green, T.J. Falloon, Pyrolite: a Ringwood concept and its current expression, in: I. Jackson (Ed.), The Earth's Mantle, Cambridge University Press, Cambridge, 1998, pp. 311–378.
[50] G. Brey, Origin of olivine melilitites: chemical and experimental constraints, J. Volcanol. Geotherm. Res. 3 (1978) 61–88.
[51] M. Arima, A.D. Edgar, High pressure experimental studies on a katungite and their bearing on the genesis of some potassium-rich magmas of the west branch of the African rift, J. Petrol. 24 (1983) 166–187.
[52] K. Mengel, D.H. Green, Stability of amphibole and phlogopite in metasomatized peridotite under water-saturated and water-undersaturated conditions, in: J. Ross (Ed.), Kimberlites and Related Rocks, vol. 14, Geological Society of Australia, Sydney, N.S.W., Australia, 1989, pp. 571–581.
[53] P. Ulmer, R.J. Sweeney, Generation and differentiation of Group II kimberlites: constraints from a high-pressure experimental study to 10 GPa, Geochim. Cosmochim. Acta 66 (2002) 2139–2153.
[54] R.H. Mitchell, S.C. Bergman, Petrology of Lamproites, Plenum Press, New York, 1991 447 pp.
[55] D.G. Pearson, D. Canil, S.B. Shirey, Mantle samples included in volcanic rocks: xenoliths and diamonds, in: R.W. Carlson (Ed.), Treatise on Geochemistry, vol. 2, Elsevier, Amsterdam, 2003, pp. 171–275.
[56] S.S. Schmidberger, A. Simonetti, D. Francis, C. Gariépy, Probing Archean lithosphere using the Lu–Hf isotope systematics of peridotite xenoliths from Somerset Island kimberlites, Canada, Earth Planet. Sci. Lett. 197 (2002) 245–259.
[57] K.J. Fraser, C.J. Hawkesworth, A.J. Erlank, R.H. Mitchell, B.H. Scott-Smith, Sr, Nd and Pb isotope and minor element geochemistry of lamproites and kimberlites, Earth Planet. Sci. Lett. 76 (1985) 57–70.
[58] F.O. Dudas, R.W. Carlson, D.H. Eggler, Regional Middle Proterozoic enrichment of the subcontinental mantle source of igneous rocks from central Montana, Geology 15 (1987) 22–25.
[59] R.W. Carlson, A.J. Irving, Depletion and enrichment history of subcontinental lithospheric mantle: an Os, Sr, Nd and Pb isotopic study of ultramafic xenoliths from the northwestern Wyoming Craton, Earth Planet. Sci. Lett. 126 (1994) 457–472.
[60] T.D. Peterson, S. Esperanca, A.N. LeCheminant, Geochemistry and origin of the Proterozoic ultrapotassic rocks of the Churchill Province, Canada, Mineral. Petrol. 51 (1994) 251–276.
[61] H.E. O'Brien, A.J. Irving, I.S. McCallum, M.F. Thirlwall, Strontium, neodymium, and lead isotope evidence for the interaction of post-subduction asthenospheric potassic mafic magmas of the Highwood Mountains, Montana, USA, with ancient Wyoming craton lithospheric mantle, Geochim. Cosmochim. Acta 59 (1995) 4539–4556.
[62] H. Mirnejad, K. Bell, Origin and source evolution of the Leucite Hills lamproites: evidence from Sr–Nd–Pb–O isotopic compositions, J. Petrol. 47 (2006) 2463–2489.
[63] S.F. Foley, Vein-plus-wall-rock melting mechanism in the lithosphere and the origin of potassic alkaline magmas, Lithos 28 (1992) 435–453.
[64] J.M. Rosenbaum, Mantle phlogopite: a significant lead repository? Chem. Geol. 106 (1993) 475–483.
[65] J.D. Vervoort, P.J. Patchett, J. Blichert-Toft, F. Albarede, Relationships between Lu–Hf and Sm–Nd isotopic systems in the global sedimentary system, Earth Planet. Sci. Lett. 168 (1999) 79–99.
[66] M. Bizimis, V.J.M. Salters, J.B. Dawson, The brevity of carbonatite sources in the mantle: evidence from Hf isotopes, Contrib. Mineral. Petrol. 145 (2003) 281–300.
[67] B.D. Taras, S.R. Hart, Geochemical evolution of the New England seamount chain: isotopic and trace element constraints, Chem. Geol. 64 (1987) 35–54.
[68] K.R. Moore, B.J. Wood, The transition from carbonate to silicate melts in the $CaO–MgO–SiO_2–CO_2$ system, J. Petrol. 39 (1998) 1943–1951.
[69] C. Dupuy, J.M. Liotard, J. Dostal, Zr/Hf fractionation in intraplate basaltic rocks: carbonate metasomatism in the mantle source, Geochim. Cosmochim. Acta 56 (1992) 2417–2423.
[70] W.R. Taylor, D.H. Green, Measurement of reduced peridotite–C–O–H solidus and implications for redox melting of the mantle, Nature 332 (1988) 349–352.
[71] G.C. Bond, P.A. Nickeson, M.A. Kominz, Breakup of a supercontinent between 625 Ma and 555 Ma: new evidence and implications for continental histories, Earth Planet. Sci. Lett. 70 (1984) 325–345.
[72] S.F. Foley, The genesis of continental basic alkaline magmas: an interpretation in terms of redox melting, Journal of Petrology Special Lithosphere Issue, 1988, pp. 139–161.
[73] F.J. Spera, Dynamics of translithospheric migration of metasomatic fluid and alkaline magma, in: M.A. Menzies, C.J. Hawkesworth (Eds.), Mantle Metasomatism, Academic Press, London, UK, 1987, pp. 1–20.
[74] W.R. Roest, S.P. Srivastava, Seafloor spreading in the Labrador Sea: a new reconstruction, Geology 17 (1989) 1000–1003.
[75] C.H. Emeleus, J.R. Andrews, Mineralogy and petrology of kimberlite dyke and sheet intrusions and included peridotite xenoliths from South-west Greenland, Phys. Chem. Earth 9 (1975) 179–197.
[76] C.E. Keen, R.C. Courtney, S.A. Dehler, M.C. Williamson, Decompression melting at rifted margins: comparison of model predictions with the distribution of igneous rocks on the eastern Canadian margin, Earth Planet. Sci. Lett. 121 (1994) 403–416.
[77] J. Eisele, M. Sharma, S.J.G. Galer, J. Blichert-Toft, C.W. Devey, A.W. Hofmann, The role of sediment recycling in EM-1 inferred

from Os, Pb, Hf, Nd, Sr isotope and trace element systematics of the Pitcairn Hotspot, Earth Planet. Sci. Lett. 196 (2002) 197–212.
[78] G.M. Nowell, D.G. Pearson, D.R. Bell, R.W. Carlson, C.B. Smith, P.D. Kempton, S.R. Noble, Hf isotope systematics of kimberlites and their megacrysts: new constraints on their source regions, J. Petrol. 45 (2004) 1583–1612.
[79] V.J.M. Salters, S.R. Hart, The mantle sources of ocean ridges, islands and arcs: the Hf-isotope connection, Earth Planet. Sci. Lett. 104 (1991) 364–380.
[80] J.S. Stacey, J.D. Kramers, Approximation of terrestrial lead isotope evolution by a two-stage model, Earth Planet. Sci. Lett. 26 (1975) 207–221.